Novel Conceptual Designs for Stopped-Rotor Aerial Vehicles and Other High-Speed Rotorcraft

Larry A. Young[1]
NASA Ames Research Center
Moffett Field, CA 94035

ABSTRACT

The objective of this paper is to present some novel vertical lift aircraft design concepts that hold potential for high-speed (greater than or equal to 400 knots) flight but still provide for efficient hover and vertical takeoff and landing capabilities. The pursuit of a high-speed rotorcraft has periodically captured the attention of rotorcraft researchers for decades. In the late 1990's to early 2000's, NASA sponsored several high-speed rotorcraft studies. A few recent works have begun to outline novel high-speed rotorcraft concepts that have been largely unexplored so far. This paper discusses four such novel concepts: two stopped-rotor concepts and two non-stopped-rotor concepts.

NOMENCLATURE

A	Rotor disk area, ft^2; $A=\pi R^2$
A_P	Stopped-cycloidal-rotor projected area, ft^2
c_R	Mean chord of rotors, ft
c_w	Mean chord of the fixed-wing of aircraft, ft
C_P	Rotor, or proprotor, or fan power coefficient, nondim.; $C_P = P/\rho A V_{tip}^3$
C_P^*	Stopped-cycloidal-rotor power coefficient, nondim.; $C_P^* = P_{Total}/\rho A_P V_{blade}^3$
C_T	Rotor, or proprotor, or fan thrust coefficient, nondim.; $C_T = T/\rho A V_{tip}^2$
C_T^*	Stopped-cycloidal-rotor thrust coefficient, nondim.; $C_T^* = T_{Total}/\rho A_P V_{blade}^2$
DOF	Degree-of-freedom, nondim.
i_N	Nacelle tilt, Deg.
i_P	Nacelle pivot, Deg.
L/D	Lift to drag ratio, nondim.
L/D_e	Effective lift to drag ratio for rotorcraft, $L/D_e = WV/P$
P	Vehicle total power,
PAX	Number of passengers, nondim.
R	Rotor radius, ft
s_{min}	Minimum offset spacing between rotors and aircraft fixed-wing, ft (m); $s_{min} > c_w/2$
s_{off}	Offset spacing between the rotors and the aircraft fixed-wing, ft
S	(Fixed-) wing planform area, ft^2
V	Cruise velocity, ft/s (m/s
W	Takeoff gross weight of vehicle, lb_f
α	Angle of attack, Deg.
β	Sideslip angle, Deg.
Γ	Wing dihedral/anhedral angle, Deg.
$\Delta D_e/L$	Delta effective drag to lift ratio, nondim.

[1] Presented at the 6th Decennial VFS Aeromechanics Specialists' Conference, Santa Clara, CA, Feb 6-8, 2024.

INTRODUCTION

Over the past several decades, the pursuit of higher cruise speed capability for vertical takeoff and landing (VTOL) aircraft, while still retaining efficient hovering flight, has long been the goal for many in the rotorcraft research community. Advances in tiltrotor aircraft have pushed the speed boundary to approximately 300 knots in level flight. NASA has been active in tiltrotor research since the 1960's, e.g., Refs. 1-9. Since the late 1980's, NASA research has waxed and waned as to high-speed rotorcraft research; however, during those times when NASA VTOL high-speed research has been active, achieving greater than or equal to 400 knots has been the general design goal. There have been numerous VTOL aircraft design configurations suggested for attaining 400 knots or greater. One of the most recent attempts to develop a high-speed rotorcraft is the DARPA SPRINT project, Ref. 10. It is not, however, merely the pursuit of higher speed that is important but, in fact, the global goal is to narrow the productivity gap between rotorcraft and commercial subsonic aircraft. Among these many proposed high-speed rotorcraft configurations are stopped-rotor designs.

Almost every rotorcraft researcher and designer at one point or the other in their careers has probably considered, to some level, the design problem of a stopped-rotor rotary-wing vehicle. It has been the elusive holy grail of many in the rotorcraft community. Two different novel stopped-rotor VTOL configurations will be discussed in this paper. Additionally, two alternate, potential non-stopped-rotor high-speed VTOL aircraft configurations will also be discussed, providing context to the relative merits of each category of high-speed rotorcraft. These novel stopped-rotor aerial vehicles will be compared to a pusher-proprotor tiltrotor and a tilt-nacelle ducted fan aircraft with one or two degrees of freedom tilt mechanisms and noncircular (oval) ducts, Refs. 11-13.

HIGH-SPEED ROTORCRAFT MISSION PROFILES AND DESIGN REQUIREMENTS

A generic set of mission profiles and design requirements will be described in this section. These mission profiles and the associated design requirements are presented in Figs. 1-2 and Tables 1-2.

Two notional mission profiles (Figs. 1-2) and sets of design requirements (Tables 1-2) are provided for first-order vehicle sizing presented later in the paper for two different "generations" of the four novel high-speed rotorcraft studied. The first generation vehicles will be consistent with UAV or small aircraft configurations; the second generation will be for larger, passenger-carrying regional aircraft.

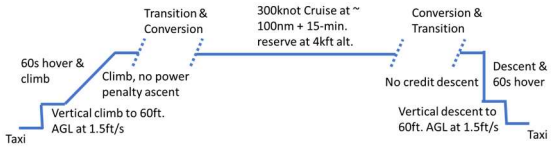

Figure 1. Mission profile for first generation vehicles (UAVs or small aircraft)

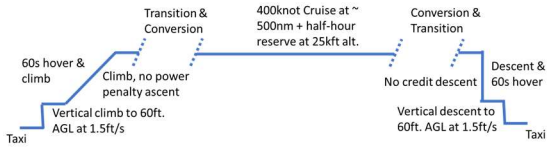

Figure 2. Mission profile for second generation vehicles (larger passenger-carrying regional aircraft configurations)

Table 1. Additional design requirements for first generation UAV/small-aircraft configurations

Payload	500 lbf
Percentage of total flight expenditure from electric motors versus turboshaft engines	10%
Reserve fuel/energy (at cruise speed and energy expenditure)	15min.
Cruise speed	300knots (506 ft/s)
Cruise altitude	4kFt.
City building rooftops, the top of parking structures, and industrial park limited-feature vertiports	VTOL
Total hover time for mission	2min. (120 sec.)
Vertical climb rate	1.5ft/s

Both Tables 1-2 reflect the inclusion of sustainable aviation objectives by requiring hybrid-electric propulsion systems for first and second generation aircraft. This is done by setting a design target goal of 10% of the total energy expended during the mission profile to be provided by battery-power. There is no requirement though for inflight generation of propulsion power through the use of turbo-electric generators. Another noteworthy aspect of Tables 1-2 is that a lower reserve power is required for the first generation aircraft than the second generation aircraft. The first generation aircraft are not required to fly at cruise speeds greater than 400knots but, instead, at more state-of-the-art (SOA) speeds of 300knots. This makes the important point that increased productivity through the use of novel aircraft may be gained even if the high-speed goal of speeds greater than 400knots is not achieved in the near-term future. In addition to the lower cruise speed requirement, the first generation vehicles have a lower total range requirement of 100nm versus the second generation vehicles' 500nm range. Finally, because it is inevitable that sustainable aviation and high-speed operation objectives will drive the resulting aircraft designs to higher takeoff gross weights than otherwise might be the case, the second generation design requirements have lower passenger count requirements than comparable lower-speed rotorcraft or non-VTOL aircraft serving the regional, passenger-carrying market.

Table 2. Additional design requirements for second generation large, passenger-carrying regional aircraft configurations

Number of PAX and Crew	50
Percentage of total flight energy expenditure from electric motors versus turboshaft engines	10%
Reserve fuel/energy (at cruise speed and energy expenditure)	30min.
Cruise speed	400knots (675 ft/s)
Cruise altitude	25kFt.
Full-featured vertiport or airport facilities	VTOL
Total hover time for mission	2min. (120 sec.)
Vertical climb rate	1.5ft/s

PROBLEMS IN COMMON THAT MOST HIGH-SPEED ROTORCRAFT CONCEPTS FACE

Why is it so hard to arrive at a satisfactory high-speed (greater than 400knots) rotorcraft? Table 3 summarizes a few of the many technical challenges that exists in general for most stopped-rotor or other high-speed rotorcraft concepts. (Note that unique technical challenges for each of the four novel high-speed rotorcraft concepts discussed in this study will also be summarized later in this paper.) The general technical challenges in Table 3 (and other

concerns) have been a key factor on why greater than 400knot rotorcraft have not been developed to date. Each of the four novel high-speed rotorcraft concepts in this study will be discussed in the context of the general set of challenges in Table 3 and their own unique technical challenges.

Table 3. General stopped-rotor and/or high-speed rotorcraft technical challenges

1.	Increased mechanical complexity and added weight to aircraft for rotor deployment/stowage mechanisms
2.	Rotor/flight dynamics and control issues associated with rotor/proprotor stopping and starting mid-flight
3.	Added profile/parasite drag, increased wetted area, and low L/D associated with stopped (non-lifting or non-propelling) rotors
4.	Added weight and mechanical complexity of auxiliary propulsion systems dedicated to high-speed cruise flight
5.	New fundamental aerodynamic investigations, system analysis tools and techniques, and conceptual design tools required to analyze truly novel high-speed rotorcraft; e.g. a new generation of airfoils from wings and rotors
6.	'Sustainable aviation' goals may or may not be achievable; hybrid-electric/turboshaft-engine systems may be too far of a reach for high-speed rotorcraft
7.	Stopped-rotor configurations (vs. non-stopped-rotor configurations) require the successful development of convertible engines (to transition from turboshaft-type to turbofan operation; this is still an open field of propulsion research and development
8.	A consistent set of missions, design requirements, and trade study analysis tools need to be developed and employed to perform reasonable analysis of alternatives between the various proposed high-speed rotorcraft concepts (both those proposed in this paper and those in the literature)

Why is it important to arrive at one or more satisfactory high-speed rotorcraft designs? One major application domain that could benefit from the successful development of high-speed rotorcraft is disaster relief and emergency response, e.g., Refs. 14-15. Another potential application domain is the use of VTOL vehicles for regional commercial air travel. As noted previously, high-speed capability would help close the gap in productivity between rotorcraft and commercial conventional takeoff and landing (CTOL) fixed-wing aircraft.

NOVEL STOPPED-ROTOR AERIAL VEHICLES

Two novel stopped-rotor aerial vehicle configurations are introduced in this paper: (1) the WING ((rotary-) Wings Integrated into New Geometry) tiltrotor aircraft and (2) the SCR (Stopped-Cycloidal-Rotor) VTOL aircraft. In both cases, the objectives of these stopped-rotor aerial vehicles would be to either increase overall flight efficiency at cruise speed and/or increase that cruise speed above the state-of-the-art.

As a part of the general discussion for all high-speed rotorcraft discussed, the following outline will be taken: a general description will be provided, the overall design space discussed, the technical challenges of the concept summarized, a brief introductory aerodynamic analysis will be presented, and then, finally, some initial first-order sizing will be provided. Aerodynamic and sizing analysis will first be presented for vehicles that meet the first generation

mission profile/requirements and then these results will also be presented for the vehicle that responds to the second generation mission profile.

WING Tiltrotor Aircraft

In contrast to previously proposed stopped-rotor tiltrotor aircraft, the rotor blades in the concept outlined in this paper are not stopped and then folded back along rotor nacelles (for tractor-type proprotors) or behind the nacelles (for pusher-type proprotors) but are instead clocked/indexed to a near-horizontal orientation whereby they become fixed "lifting wings" providing partial lift for the vehicle in high-speed cruise. The result, when the rotors are stopped, is a tandem- or joined-wing vehicle wherein the aft wing is the primary wing and the stopped-rotor blades become the forward wing; refer to Fig. 3a-b. (Joined-wing tiltrotor aircraft have been studied before, e.g., Refs. 16-18, but not as stopped-rotor configurations.)

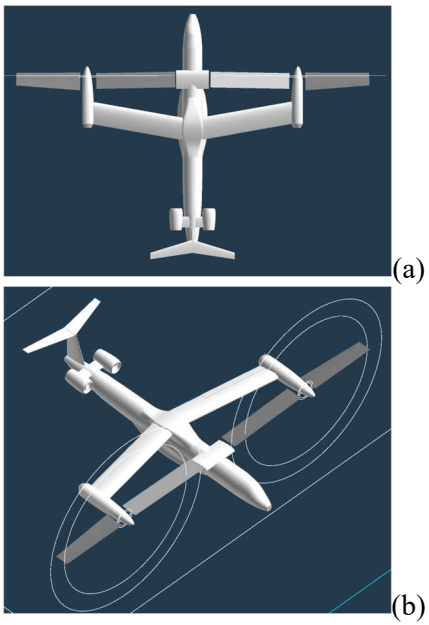

Figure 3. Notional WING stopped-rotor tiltrotor aircraft: (a) top/planform and (b) isometric views

The baseline configuration's rotor blades are untwisted and employ only symmetrical blades (refer to complementary discussion related to the "Flex" vehicle concept outlined in Ref. 11) to allow the blades to be feathered into the "wind" as the rotors are slowed and ultimately stopped. Advances in smart materials, as applied to the rotors, might however make it feasible to incorporate embedded flaps and/or indexed-tips to tailor the effective twist of the blades for hover and then "un-twist" the blades for high-speed forward-flight and their ultimate stopping and stowing. The concept includes the provision for a telescoping canard-like blade snubber/damper to restrict the motion of the inboard blades and, thereby, providing two-point support; refer to Fig. 4.

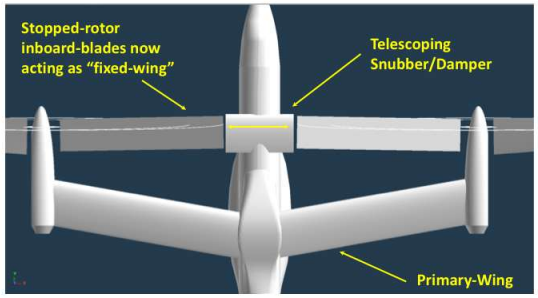

Figure 4. Close-up planform view of primary fixed wing and the stopped rotors as auxiliary wings, and a telescoping snubber/damper to capture stopped rotors, resulting in a continuous span

Given the whirl-flutter experience of the XV-3 tiltrotor aircraft, proposing a two-bladed-rotor tiltrotor aircraft might seem to be counterintuitive to the goal of a high-speed tiltrotor aircraft. However, if asymmetric rotor blades (particularly asymmetry as regards the relative blade-to-blade azimuthal phasing) are employed then it might be possible to implement the WING concept with more than two-bladed rotors. Finally, the XV-3 two-bladed rotor experience is not

generally applicable as the WING rotors would be stopped (and captured/retained by a telescoping snubber/damper) before the rotor instabilities for the two-bladed rotor were manifested at higher forward-flight speeds.

With the rotors stopped, a tandem- or joined-wing vehicle configuration would result because of the primary-wing vertical placement with respect to the vehicle fuselage and/or the rotor nacelle/pylon nacelle-tilt axis vertical offset with respect to the primary-wing mean chord line. This question (tandem- versus joined-wing) is one of the key vehicle configuration questions that will be investigated with CFD.

Slowed- and stopped-rotors can be modeled in a mid-fidelity CFD software tool called RotCFD; refer to Refs. 19-20. RotCFD can successfully model the slowed- and stopped-rotors with its "unsteady" rotor option (a 'virtual blade' or lifting-line-like momentum sources) with very small (near-zero) prescribed rotor RPMs. Further, dissimilar blades can be modeled, if need be, by overlaying multiple rotors (with one or more blades) exactly over each other to form a final aggregate rotor. These unique modeling features are in addition to the graphic user interface – and the automated gridding options built into the tool – allow for quick modeling and computations of complex vehicle configurations. Finally, RotCFD is a RANS solver that uses either the 'realizable' or standard kappa-epsilon turbulence model and has built in incompressible and compressible solvers. The incompressible flow solver uses the Reynolds Averaged Navier-Stokes equations; the compressible solver is based on the mass-weighted Favre Averaged Navier-Stokes equations. Boundary-layers cannot be modeled directly within RotCFD but are, instead, modeled using wall functions that model the near-wall log layer, the buffer layer, and a viscous sub-layer. These modeling features and capabilities make RotCFD a particularly useful tool to perform this general type of high-speed rotorcraft study.

Figure 5 is a generic first-order plot of tiltrotor delta-effective-drag-to-lift ratio (Delta-De/L) as the proprotors are being slowed down from nominal cruise rpm to near-zero rotational speeds.

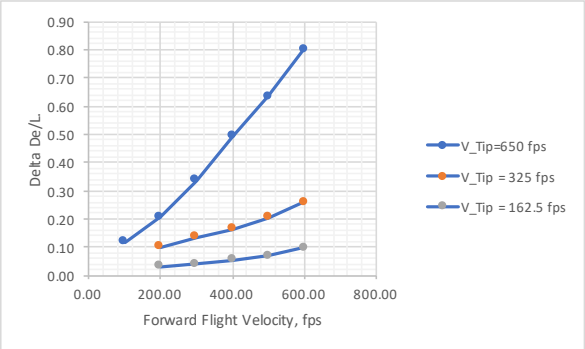

Figure 5. Delta-D_e/L effect on vehicle forward-flight performance, with the lifting-rotors being trimmed in the zero-thrust state

Figure 6 is a notional configuration for UAV or small aircraft 'first generation' WING vehicle. The vehicle is shown in its cruised stopped-rotor-configuration and surface pressures; velocity magnitude isosurfaces, and rotor disk differential pressure distributions are shown. The main (aft) fixed wing is constant chord with aspect ratio is AR=8 and the total wing planform area is S=200 ft^2. (This is the same wing aspect ratio and wing planform area as used for the notional first generation PPT aircraft and the THRUST modular technology demonstrator discussed later in the paper.) The (forward) stopped-rotor 'wing' has a slight taper and an effective wing planform

area of S=106 ft^2; this gives a total stopped-rotor total tandem wing assembly planform area of S=306 ft^2. This wing geometry was selected prior to the sizing analysis presented later in this paper.

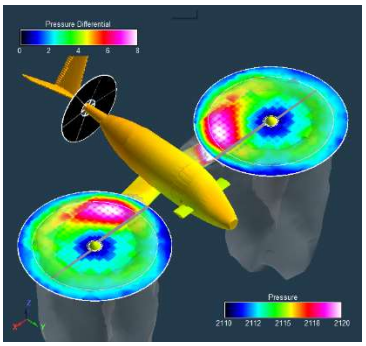
(a)

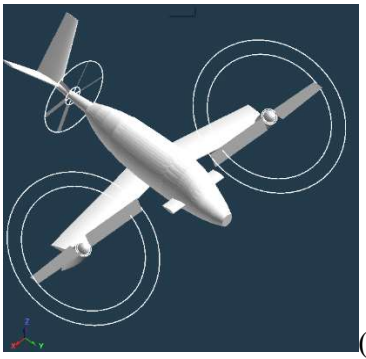
(b)

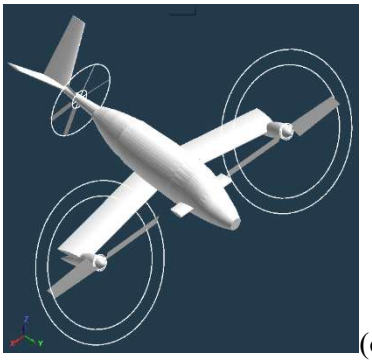
(c)

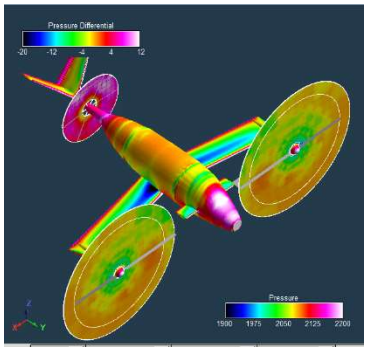
(d)

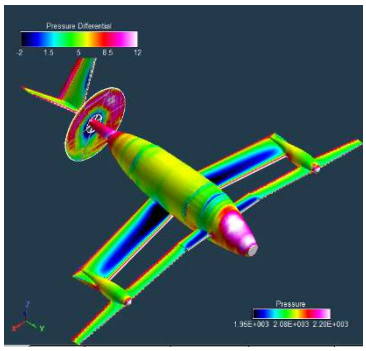
(e)

Figure 6. First generation WING aircraft through all phases of flight and stopped-rotor conversion: (a) helicopter-mode hover; (b) early transition mode; (c) late transition mode; (d) pre-stopped-rotor conversion (low rpm rotating blades); (e) cruise stopped-rotors (rear-mounted pusher propeller is used for cruise propulsion)

Figure 7 illustrates an angle of attack (AOA) sweep (at a forward flight speed of 250knots or 422ft/s) of the first generation WING vehicle. Body surface pressures are presented for these various angles of attack. Both the aft (fixed-) wing and the forward (stopped-rotor) wing upper surface suction pressures – and their increase with AOA – can be seen in the figures. The WING vehicle sees roughly a doubling of the total wing wetted area (over that of the aft fixed-wing) when the rotor blades are stopped and clocked/indexed into position.

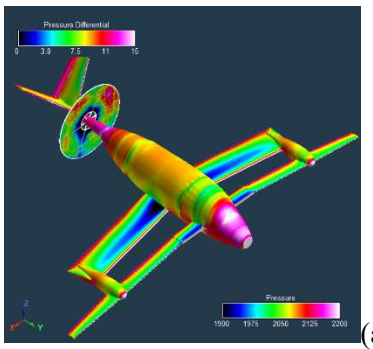
(a)

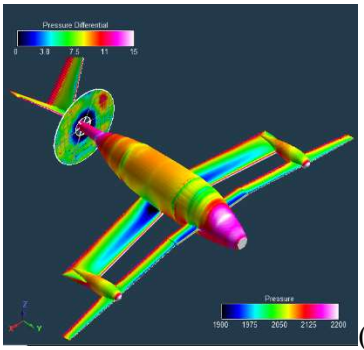

(b)

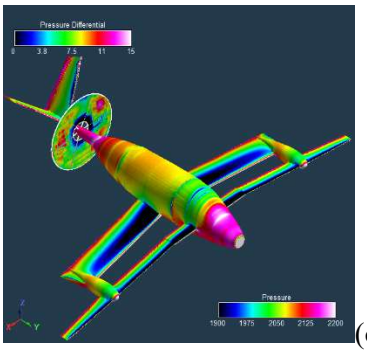

(c)

Figure 7. Body surface pressures for first generation WING vehicle: (a) AOA=2Deg.; (b) AOA=4Deg.; (c) AOA=6Deg.

Figure 8 presents an initial lift-to-drag ratio trend with vehicle lift coefficient for the first generation WING vehicle. (RotCFD solutions likely hadn't totally converged for some of cases presented but the near-maximum L/D is probably approximately accurate.) The Fig. 8 results indicate that there is an influence of the wing anhedral or dihedral angles on the overall vehicle L/D. This is because the induced velocities from the forward (stopped-rotor-blade) wing can significantly influence the aft (main fixed-) wing aerodynamic loading. The relative magnitude – and influence on the aft wing – and distribution of the forward wing induced velocities (downwash) is partly governed by the relative vertical spacing of one wing relative to the other, which in turn is governed by the anhedral/dihedral angles of the forward wing.

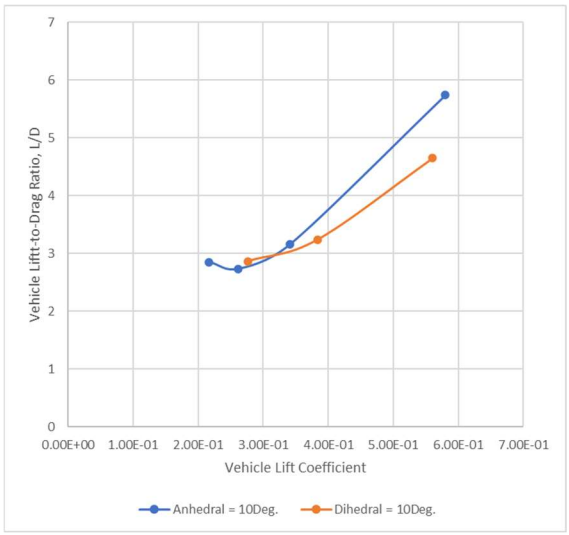

Figure 8. Lift-to-drag ratio as a function of vehicle lift coefficient for (stopped-rotor-blade anhedral and dihedral angles) first generation WING

Figure 9 is a representative nondimensional Q-criterion isosurface sample result of a stopped-rotor tiltrotor model at a forward-flight velocity of 400knots or 675ft/s, an angle-of-attack of 2 Deg., and the rotors stopped (V_{Tip}=0.0001ft/s) forming a tandem-wing or joined-wing "fixed-wing" cruise vehicle configuration. The trailed vortices from the stopped rotor "fixed-wing" surfaces and the horizontal tail can be seen in Fig. 9.

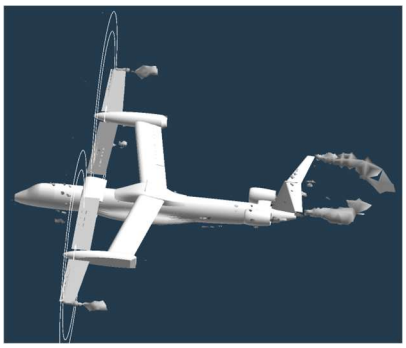

Figure 9. Rotors stopped in "stowed" cruise configuration and acting as lifting wings; nondim. Q-criterion isosurface; AOA=2 Deg.

A key risk for the WING concept is that there could be too much overall wetted area resulting from the forward wing (aka stopped-rotors) and the rear wing, thus resulting in too high skin friction drag in high-speed cruise for the aircraft. This, then, entails an interesting vehicle aerodynamic optimization challenge: minimize overall fixed-wing planform area and rotor radii and solidity while balancing "aeroperformance" (aerodynamic performance) in all phases of flight, i.e., hover, transition/conversion, and cruise. Even if an optimized aerodynamic L/D efficient solution is elusive for a stopped-rotor and wing tandem assembly geometry, though, then the concept is successful if the general cruise speed increase capability is achieved. One additional aerodynamics area to explore for the WING concept is the possible use of multi-element wing airfoil lift augmentation devices to generate increased lift (for potentially smaller fixed-wings) during transition/conversion. These wing lift augmentation technologies could include slats/slots and segmented flaps; tangential-injection-blowing lift devices such as blown-flaps might also be valuable.

A partial list of pros, cons, and technical challenges in developing the WING stopped-rotor vehicle configuration are noted in Table 4.

Table 4. Pros, cons, known unknowns, and technical challenges for WING aircraft concept

Pros:
1. Novel approach to the 'stowed rotor' problem for stopped-rotor configurations
2. Dual-purpose utility of the rotors becoming forward tandem 'wings' when stopped; potentially the most efficient weight savings approach to a stopped-rotor configuration given this multifunctional use of the rotors/'wings'
3. Potential for defining an optimized tandem/joined-wing assembly (when rotors are nonrotating and indexed into stopped position) for improved aerodynamic efficiency, L/D
4. Thinner fixed-wings could be used as potentially the stopped-rotor tandem/joined-wing assembly might have higher overall bending/torsion stiffness
Cons:
1. Increased 'wing' area and profile drag for overall effective tandem wing assembly in high-speed flight
2. High (rotor blade) wing bending moments and stresses and strains due to the thin, high-aspect-ratio, nonrotating blades being subjected to cruise aero loads without centrifugal stiffening
3. Increased control system complexity to trim nonrotating blades to wing-like pitch-angles; this stopped-rotor cruise trim requirement would be in addition to conventional rotor/proprotor swashplate control system requirements; a hub gimbal lock-out mechanism would have to be developed
4. A low-rpm transmission/clutch system would be required to be developed to slowly index azimuthally the (near-) nonrotating blades into their wing-like 'stowed rotor' tandem-wing configuration
5. Low/zero twist blades and (near-) symmetrical blade airfoils – and possibly constant chord blades – would have to be used for the WING rotors/proprotors; this might be necessary to yield acceptable incremental L/D contributions from the stopped rotors in cruise
Known Unknowns:
1. Design of a snubber set of canards to capture two of the nonrotating blade tips to increase the overall stiffness of the now wing-like assembly; the resulting tandem/joined-wing assembly bending/torsion stiffnesses need to be analytically evaluated

2. Defining variable rpm gearbox system (or propulsion concepts, including possibly hybrid-electric systems) to enable efficient transfer of power to the rotor systems through an extremely wide range of rpms to enable stopped-rotor transition/conversion
3. Design of a means of indexing nonrotating blades into position to be locked down by snubber canards; this could be accomplished by a stepper-motor, encoder, and the clutch auxiliary system (for each rotor) or possibly could be accomplished by actuated servo-flaps on the (nonrotating) blade tips
4. Design of an acceptable propulsion approach using cruise airplane-mode propulsive turbofan engines and turboshaft-engine to drive the rotors/proprotors in low-speed helicopter-mode
Technical Challenges:
1. Defining an optimized tandem/joined-wing arrangement for when blades are stopped and indexed in position for maximum L/D
2. Defining weight estimation methodologies compatible with WING concept
3. Refine overall conceptual design to perform analysis of alternatives of WING versus other stopped-rotor and high-speed rotorcraft configurations to determine the best approach for a given set of missions, e.g., a comparison of WING versus folding tiltrotor concepts (which has been proposed several times since the 1960's)
4. The WING concept needs to be demonstrated experimentally, even if only with scaled wing tunnel test models
5. WING has many of the same aero, mechanical, and tech challenges of the older folding tiltrotor concepts (but without the added complexity of the blade folding mechanism and the unique aerodynamic and dynamic nature of the folding and unfolding process)

The overall WING stopped-rotor aerodynamic design trade space (with respect to the (stopped-rotor) tandem wing assembly configurations) will now be discussed. Examples of other arrangements for a WING tandem assembly are illustrated in in Fig. 8a-d. Depending on whether the main fixed-wing is high-, mid-, or low-wing mounted, a series of different combinations of (stopped-rotor-) wing anhedral and dihedral angles can be defined. Additionally, different combinations of sweep angles for both the main fixed-wing and the (stopped-rotor-) wing can be defined and explored for possible aggregate aerodynamic benefit.

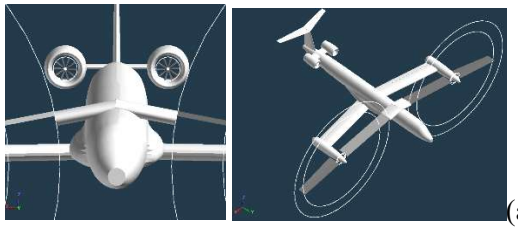
(a)

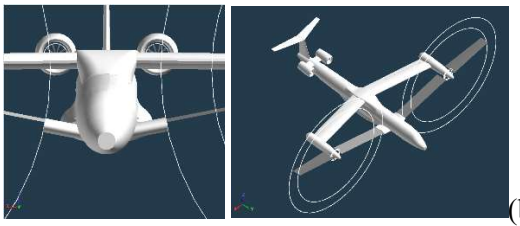
(b)

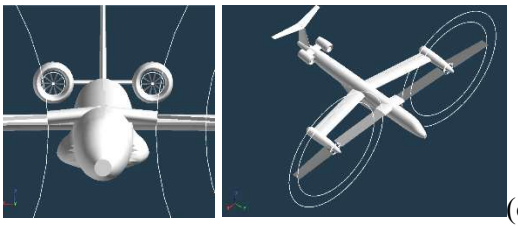
(c)

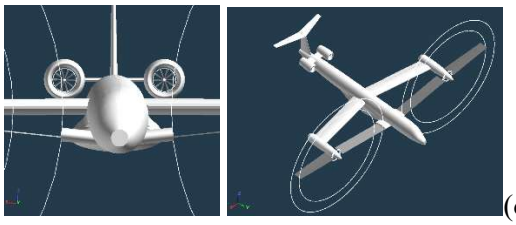
(d)

Figure 10. Other tandem (rotor) wing assembly arrangements for WING concept: (a) anhedral, (b) dihedral, (c) mid-wing with anhedral, and (d) mid-wing with dihedral

Even three-bladed configurations are viable if asymmetric azimuthal (fixed, not dynamic) indexing is employed for smaller/thinner blades used for the forward stopped-rotor 'wing' (i.e., closer angular spacing between the two smaller blades). Refer to Fig. 11a-b as an example. The use of asymmetric rotor blades (both asymmetric from a planform perspective as well as azimuthal angle placement) is a largely unexplored area of rotor aeromechanics research. The most extreme version of asymmetric rotor blades is the work in the 1960's on one-bladed rotor systems; however, there is much more that could be explored in terms of asymmetry in rotorcraft design; see, for example, Ref. 21.

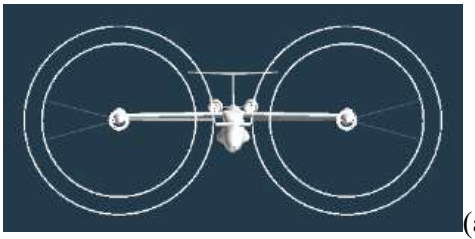

(a)

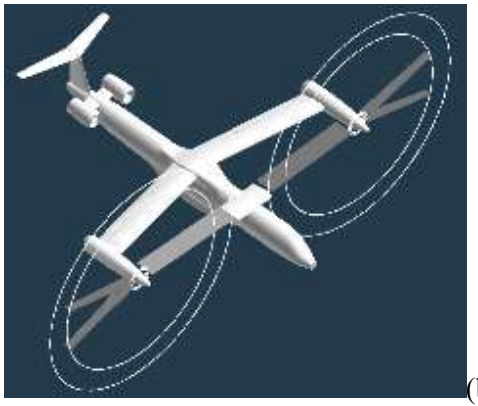

(b)

Figure 11. Three-bladed rotors can be used as forward 'wings' when the WING rotors are stopped (if asymmetric rotors are employed)

Figures 10 and 11 are just a brief illustration of the complex design trade space in simply defining the stopped-rotor wing tandem assembly arrangement from just a high speed cruise aerodynamic and aeroperformance perspective. This design space (some of the tandem assembly geometry parameters given by the array G) is also summarized in Eq. 1 below.

$$G = \begin{bmatrix} -15 \le \Lambda_{Aft\ Wing} \le 15 \\ s_{min} \le |s_{off}| \\ |\Gamma| \le acos\left(h_{cabin}/R_{large}\right) \\ 0 \le R_{small}/R_{larg} \le 1 \\ 0 \le \sigma A/S \le 2 \\ N_{blades} \end{bmatrix} \quad (1)$$

Some preliminary work related to exploring the stopped-rotor and fixed-wing geometry trade space for best aeroperformance efficiency is briefly highlighted Fig. 12. The L/D results of Fig. 12 are based on a combined 'strip theory' and RANS methodology; this methodology is outlined, in general, in Ref. 22. This work is only the initial steps in exploring a large trade space. However, these preliminary results suggest that the stopped-rotor anhedral or dihedral angles do have an influence on aggregate tandem wing assembly L/D, with anhedral angles showing a more beneficial effect.

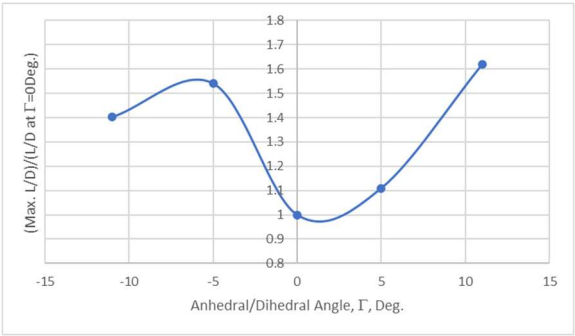

Figure 12. Initial tandem wing (stopped, nonrotating blades forward of fixed-wings) predictions using hybrid 'strip theory' within RotCFD: lift-to-drag ratio curve (normalized with respect to max L/D at Γ=0Deg.

CFD predictions of the second generation WING with the nonrotating blades fully-blade-resolved in the RANS CFD solver are shown in Figs. 13-14. The fuselage and fixed-wing geometry are based upon the NASA LCTR2 reference design, Ref. 23.

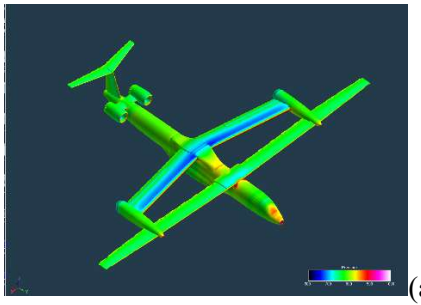
(a)

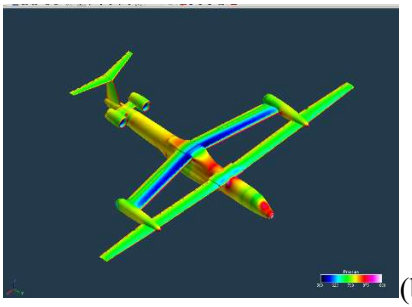
(b)

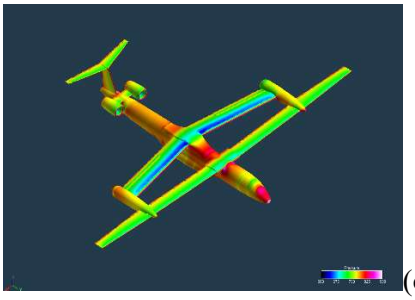
(c)

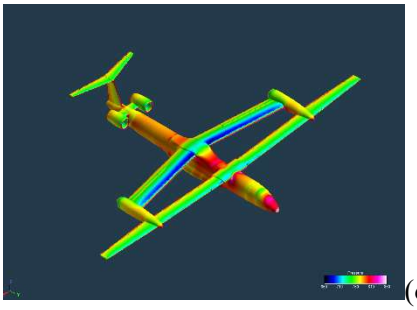
(d)

Figure 13. Surface pressure of the second generation WING (stopped-rotor-dihedral of 2 Deg., altitude of 25kft, and V=675ft/s or 400knots): (a) AOA=0 Deg.; (b) AOA=2 Deg.; (c) AOA=4 Deg.; (d) AOA=6 Deg.

Figure 14 presents a series of body surface pressures for the second generation vehicle with an alternate stopped-rotor dihedral of 11Deg.

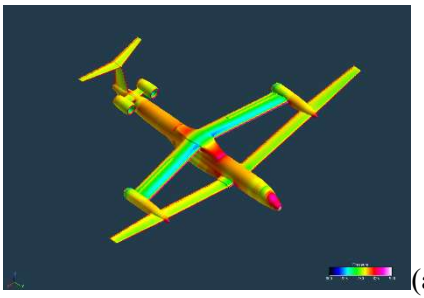
(a)

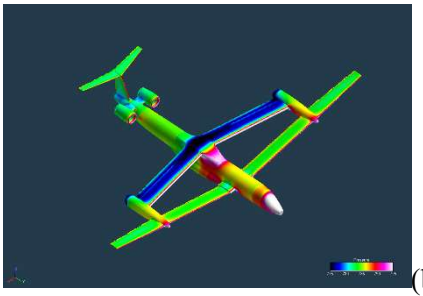
(b)

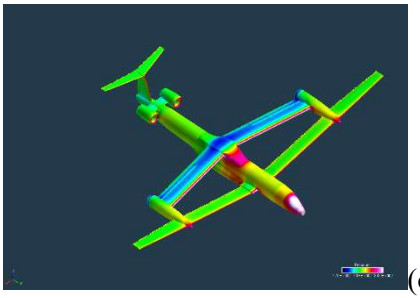
(c)

Figure 14. Surface pressure of the second generation stopped-rotor WING full-vehicle configuration (stopped-rotor-dihedral of 11 Deg., altitude of 25kft, and V=675ft/s or 400knots): (a) AOA=0 Deg.; (b) AOA=2 Deg.; (c) AOA=4 Deg

Unfortunately, premature wing stall was predicted in Fig. 14 results for angles of attack greater than two degrees. This is a modeling issue that needs to be addressed in the future; it is probably a combination of a number of factors including coarse CAD modeling of the vehicle wings (resulting in some faceting and/or uneven surfaces), aerodynamic issues related to the relatively

thick wings (21-24%) modeled, increased importance of the compressibility effects at the M~0.68 condition being explored, and, finally, the need for improved gridding refinement.

A first-order sizing analysis has been performed for both the first and second generation WING aircraft configurations and their associated mission profiles and design requirements. The results of these sizing analyses are presented in Tables 5-6. These sizing analyses leverage work for long-range hybrid-electric (conventional tube-and-wing and blended-wing-body) tiltrotor aircraft detailed, in part, in Ref. 24.

It is the novel nature of many of the high-speed rotorcraft concepts presented in this study that makes it difficult to arrive at satisfactory weight estimates of the unique hardware or mechanical systems inherent in each of these concepts. This reinforces the key point in this sizing discussion that the following work can only be considered first-order (and therefore not as accurate as weight estimates for aircraft that have a historical database of weight information). As these concepts mature and proof-of-concept and/or scaled prototype systems are developed, then more accurate weight estimation methods will be derived.

The weight estimation considerations used for the WING tiltrotor aircraft are as follows. First, most mechanical system mass estimation is equivalent to that of conventional tractor-proprotor tiltrotor estimates/estimation methodology. Second, convertible engine mass and performance estimation (an engine that converts during operation from a turboshaft to turbofan engine, and back again) is particularly challenging for stopped-rotor aircraft conceptual design work. This is because, despite of decades of work in this area, there are no production engines of this type (just paper engines or prototypes, e.g., Refs. 25-26). As a side note, it is this lack of a production convertible engine that might open (justify) an expanded use of hybrid-electric propulsion technology for stopped rotorcraft vehicles. The approach taken in this paper's (ad hoc) weight estimation analysis for nascent convertible engines is as in the below equation.[2]

$$W_{CE} = (W_{TSE} + (2 - \delta_F)W_{TFE})$$

$$1 \leq \gamma_F \leq 2$$

(2a-b)

Where in the above equation, δ_F is a 'tech factor' or 'calibration factor' used to define, in this case, a qualitative assessment of whether a convertible engine will be more turboshaft- or turbofan-like in terms of weight. In the worst case, $\delta_F = 1$, the weight estimate would be for the two engine types to both be installed on the aircraft as

[2] This approximate weight sizing methodology for arriving at weight estimates for hybrid systems (those systems that draw upon hardware/technologies from different vehicle types and R&D communities) is a reasonable general approach for first-order sizing and systems analysis. This approach, for example, was taken for amphibious VTOL vehicle sizing in Ref. 27. This approach has also been taken for hybrid air/ground mobility systems, Refs. 28-29. This hybrid system weight estimation approach can be generalized as: $W_{HS} = W_{S_0} + \sum_{i=1}(2 - \delta_{F_i})\, W_{S_i}$ where W_{HS} is overall hybrid system weight estimate and W_{S_0} is the primary individual system and W_{S_i} are the secondary or auxiliary system weight estimates that help capture or definitize the added hybrid nature of the overall system. Note that $1 \leq \delta_{F_i} \leq 2$.

independent propulsion systems. The weight of the convertible engine is given by W_{CE}. The weight of a turboshaft engine sized for max 'helicopter mode' power is W_{TSE}. And the weight of a turbofan engine sized for maximum airplane power is W_{TFE}. (Turbofan engine information and sizing can be found from Refs. 41-42.) For the purposes of this study, it is assumed that δ_F~1.5-1.75. This tech/calibration factor can be adjusted as more future engineering work is performed on convertible engine assessments. Third, after the convertible engine estimation, there will be modest increases (assume ~10% increase over conventional ~300knots tiltrotor baseline) in control system weights to account for setting nonrotating rotor collective pitch trim to angles consistent for their stopped-rotor effective AOA positions. Fourth, a delta increase (assume a 5% increase over the baseline tiltrotor aircraft) is added to fuselage weight to reflect the addition of the canard snubbers. Fifth, small increases in drivetrain weight (~5%) are made to account for the 'indexing' mechanism to move/index the stopped-rotor blades into (their azimuthal) position to be grabbed by telescoping canard snubbers and thus forming the cruise tandem/joined assembly of (nonrotating) blades and wings. Sixth, an increased tail elevator range and greater overall tail volume will be required to accommodate the large delta change in (tandem) wing planform area; this will likely result in a small increase in the empennage weight and, therefore, overall fuselage weight (this delta weight is assumed included in the above 5% fuselage weight increase). Seventh, the fixed equipment weight is reduced by the correction factor equal to PAX/90. Eighth, the wing weight has been reduced by a factor of 18/24, or 3/4, to reflect going to a thinner 18% wing than the typical 21-24% thick wings for conventional tiltrotor aircraft. Finally, other than the above noted exceptions, in terms of the weight estimation methodology approach taken, the WING aircraft (and the pusher-proprotor tiltrotor (PPT) concept for that matter) can use most of default conventional tiltrotor aircraft sizing methodology (for example, the methodology detailed in Ref. 24).

The results of this first order sizing analysis for the WING concept, for the first and second generation mission profiles and requirements, are presented in Tables 5 and 6.

Table 5. First-order vehicle sizing for first generation (UAV/small-aircraft) WING aircraft concept ($E_{Battery}/E_{Total}$, = 0.09)

Main Rotor Disk Loading	20.32	lbf/ft^2
Main Rotor Radius	4.83	ft
Number of Blades	2.00	Nondim.
Main Rotor Solidity	0.12	Nondim.
Main Rotor Tip Speed	781.53	ft/s
Nominal (Mean) Airplane-Mode Cruise Wing Loading	107.86	lbf/ft^2
Wing Span	12.54	ft
Number of Electric Motors per Rotor	1.00	Nondim.
Hover Power	277.82	Hp
Advance Ratio	0.21	Nondim.
Nominal Helicopter-Mode Forward Flight Power	139.75	Hp
Vehicle Effective Lift over Drag in Airplane-Mode Cruise	6.00	Nondim.
Nominal (Mean) Airplane-Mode Cruise Power	549.65	Hp
Energy from Battery over Total Mission Energy	0.09	Nondim.
Prescribed Fraction of Power Delivered by Electric Motors in Hover versus Turboshaft Engines	0.25	Nondim.
Prescribed Fraction of Power Delivered by Electric Motors in Helicopter-Mode Forward Flight versus Turboshaft Engines	0.25	Nondim.
Prescribed Fraction of Power Delivered by Electric Motors in Airplane-Mode Cruise versus Turboshaft Engines	0.00	Nondim.
Payload (an/or Combined Passenger(s) and Crew)	500.00	lbf
Total Weight of Rotors	17.27	lbf
Fuselage Weight	17.45	lbf
Wing Weight	1134.19	lbf
Total Convertible Engines and Drive Train Weight	403.77	lbf
Total Fuel Weight	99.20	lbf
Total Battery Weight	340.14	lbf
Total Electric Motor Weight	136.66	lbf
Total Fixed Equipment Weight	106.13	lbf
Total TOGW =	2754.81	lbf

Because of NASA interest in sustainable aviation, all high-speed rotorcraft configurations were sized with a common set of requirements that during hover and low-speed helicopter-mode forward flight 25% of

total rotor shaft power is required to be provided by electric motors (through a two-input-shaft gearbox) supplied by batteries. The remaining 75% would be provided by a mechanical drive train driven by a turboshaft or convertible engine. In total, this typically results in approximately 5-10% of the total expended energy during a mission to be supplied by batteries. Alternate hybrid-electric propulsion approaches are not considered in this paper. Therefore turbo-electric generators – and their weight – are not included in the propulsion system weight estimates. Attempting to develop a high-speed rotorcraft that is also responsive to sustainable aviation concerns is a major design challenge and one that is largely unexplored till now.

Table 6. First-order vehicle sizing for second generation (large, passenger-carrying regional) WING aircraft concept

Main Rotor Disk Loading	20.32	lbf/ft^2
Main Rotor Radius	30.84	ft
Number of Blades	2.00	Nondim.
Main Rotor Solidity	0.12	Nondim.
Main Rotor Tip Speed	781.53	ft/s
Nominal (Mean) Airplane-Mode Cruise Wing Loading	98.63	lbf/ft^2
Wing Span	83.15	ft
Number of Electric Motors per Rotor	1.00	Nondim.
Hover Power	11335.26	Hp
Advance Ratio	0.21	Nondim.
Nominal Helicopter-Mode Forward Flight Power	5701.74	Hp
Vehicle Effective Lift over Drag in Airplane-Mode Cruise	10.00	Nondim.
Nominal (Mean) Airplane-Mode Cruise Power	17940.68	Hp
Energy from Battery over Total Mission Energy	0.07	Nondim.
Prescribed Fraction of Power Delivered by Electric Motors in Hover versus Turboshaft Engines	0.25	Nondim.
Prescribed Fraction of Power Delivered by Electric Motors in Helicopter-Mode Forward Flight versus Turboshaft Engines	0.25	Nondim.
Prescribed Fraction of Power Delivered by Electric Motors in Airplane-Mode Cruise versus Turboshaft Engines	0.00	Nondim.
Payload (an/or Combined Passenger(s) and Crew)	12500.00	lbf
Total Weight of Rotors	13721.65	lbf
Fuselage Weight	23308.91	lbf
Wing Weight	6766.89	lbf
Total Convertible Engines and Drive Train Weight	19232.65	lbf
Total Fuel Weight	12363.84	lbf
Total Battery Weight	14028.39	lbf
Total Electric Motor Weight	3843.59	lbf
Total Fixed Equipment Weight	7251.27	lbf
Total TOGW =	113017.20	lbf

Stopped-Cycloidal-Rotor (SCR) Aircraft

Cycloidal rotor concepts have been proposed for decades. Recently, cycloidal rotor vertical lift aerial vehicles have met some success in the form of micro air vehicles. In 2016, a student internship project within the NASA Ames Aeromechanics Office examined, to a first order, the use of various stopped-rotor cyclocopter configurations for the possible exploration of the mid- to lower- atmospheric altitudes of the planet Venus; see Ref. 30. This paper will examine a specific type of stopped-cycloidal rotor vehicle that may be scalable from small UAVs to larger, passenger-carrying regional high-speed VTOL aircraft; refer to Fig. 15.

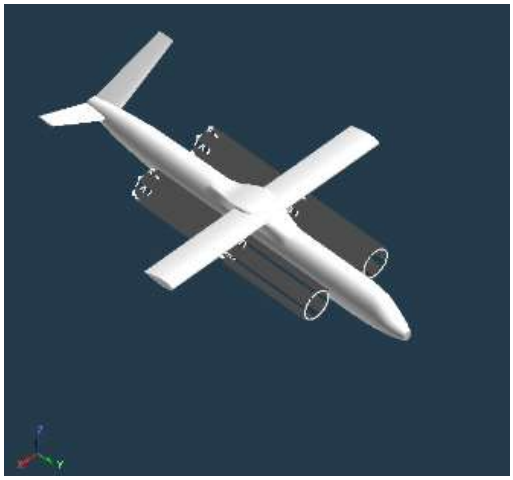

Figure 15. Isometric view of stopped rotor cycloidal vehicle

Table 7 is a partial list of the pros, cons, known unknowns, and technical challenges for stopped-cycloidal-rotor vehicles. In a general comparative sense, there are a greater number of known unknowns for SCR aircraft. The WING aircraft concept has a lot of common technical challenges with respect to folding-proprotor tiltrotor concepts, which have been long-studied. On the other hand,

only recently has modest-sized (dozens to hundreds of pound-force) cycloidal rotor technology for aircraft been developed and demonstrated, e.g. Ref. 31. It is a big leap to advocate for large passenger-carrying aircraft from the current SOA. Nonetheless, if a large passenger-carrying SCR were indeed viable, it could potentially be the foundation to develop a wide-ranging class of VTOL vehicles and missions.

Table 7. Pros, cons, known unknowns, and technical challenges for Stopped-Cycloidal-Rotor aircraft concept

Pros:
1. The proposed stopped-cycloidal-rotor configuration theoretically addresses in an efficient manner the 'stowed-rotor' problem for high-speed cruise flight for stopped-rotors
2. The yawed flow over the rotor blades with increasing vehicle forward flight speed is benign from an aerodynamic perspective
Cons:
1. It may be too big of a conceptual leap to convince people that one can go from flight-demonstrated cycloidal rotor micro-air-vehicles to passenger-carrying regional aircraft
2. This vehicle configuration might not be suitable for military missions, only civilian/commercial, because of the low ground clearance of the cycloidal rotors
3. Centrifugal loading on large-scale rotor blades might be quite challenging from a mechanical system design perspective
4. The rotating 'stators' for holding the blades in position (at both ends of the blades) have to be stiff, low drag, and capable of supporting actuators and control hardware to effect sinusoidal blade pitch angle input on a once per revolution basis; however, a sinusoid input is not necessarily optimal for cycloidal rotors, a more pulse/step function input might be more appropriate when the blades are at their 'rise' and 'fall' positions during one revolution
5. Auxiliary propulsion for high-speed cruise is required, like other stopped-rotor configurations; this entails the development of convertible engines or distributed hybrid-electric propulsion to efficiently integrated lifting cycloidal rotors with auxiliary propulsors
Known Unknowns:
1. Sizing analyses for large passenger-carrying stopped-cycloidal rotors are still in very early stages of development, with an accompanying large amount of performance and weight estimation uncertainty
2. Cycloidal rotor and wing and fuselage aerodynamic interactions are unlike rotor/wing/fuselage interactions for other rotorcraft configurations; such SCR aero interactions need to be studied in detail both computationally and experimentally
Technical Challenges:
1. Stopped-cycloidal-rotor aircraft aerodynamics and rotor wakes is largely unexplored for all regimes of flight: hover, transition/conversion, and cruise
2. Radically different flight control systems (as compared to conventional helicopter/tiltrotor collective and cyclic swashplate control) need to be designed for SCR aircraft
3. The optimal combination of cycloidal rotors (and their size, loading, and airfoil/blade-planform characteristics) are still largely an open question; current work has explored a couple different approaches, but considerably more work needs to be performed to reach a reasonable conclusion as to such an optimal SCR rotor arrangement

Figures 16-18 illustrate an example of a complete aircraft (for a simple first generation vehicle geometry) mid-fidelity CFD flow field predictions for various operating conditions. Note that the cycloidal rotor axis (and therefore blade span) is

aligned with the longitudinal axis of the aircraft. This is the key novel aspect of the stopped-cycloidal-rotor configuration to be explored. (Note that the shown vehicle configuration in Fig. 16 is not consistent with the first generation mission profile of Fig. 1; the configuration shown in Figs. 16-18 is early proof-of-concept work to demonstrate that the RotCFD software tool could model cycloidal rotors and SCR aircraft overall.)

The aeroperformance approach taken in the first and second generation SCR sizing analysis is to use simple surrogate rotor performance models derived from the above noted RotCFD predictions and to use those surrogate models in the sizing analysis. The general form of the surrogate model is

$$P = f(T, V_{blade}, \Delta\theta_{blade}, \mu, \delta_I) \tag{3}$$

Where in the above equation: P is SCR power; T is the total SCR cycloidal rotor thrust; V_{blade} is the rotational speed of the cycloidal rotor blades, $\Delta\theta_{blade}$ is the magnitude of the half-peak (assumed sinusoidal in this paper) azimuthal variation of the blade pitch angle, μ is the SCR advance ratio, $\mu = V/V_{blade}$; δ_I is an aerodynamic interference factor to account for rotor-on-rotor and airframe-on-rotor interference effects.

The SCR total rotor power surrogate model form could be

$$P = \delta_I C \Delta\theta_{blade} V_{blade}^2 g(\mu, T) \tag{4a}$$

Where for the purposes of this study

$$g(\mu) \propto 1 + c\mu \tag{4b}$$

Alternatively, the simplest surrogate model (and the one used in the first-order sizing analysis performed in this paper) is

$$P = aT^b(1 + c\mu) \tag{4c}$$

And a, b, c, and C are empirical regression coefficients derived from the RotCFD SCR predictions shown below. A set of regression coefficients were developed for the first generation vehicle and a second set of regression coefficients were derived for the second generation vehicle.

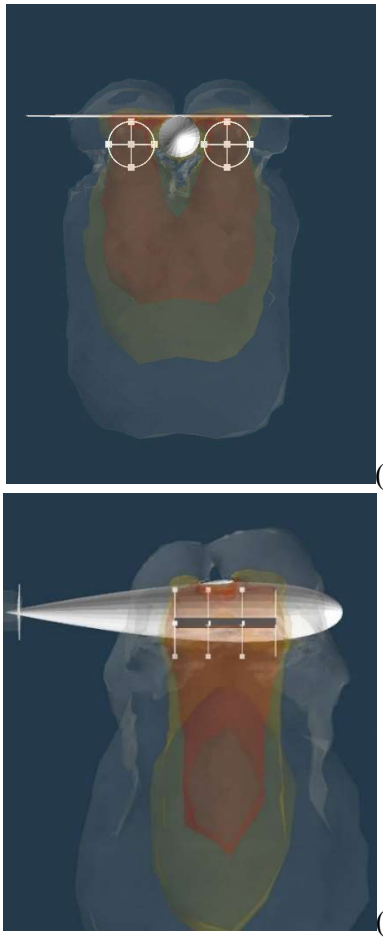
(a)

(b)

Figure 16. Hover stopped-cycloidal-rotor VTOL vehicle rotor wakes (isosurfaces of velocity magnitude): (a) front and (b) side views

Instead of cylindrical, contracted wake of conventional helicopters and tiltrotors, the wake of a SCR is a quasi-rectangular wake. It, just like a conventional rotor's wake, does skew backwards as forward flight velocity is increased. These SCR hover and forward flight wake characteristics can be seen in Figs. 16-17. At high-enough forward flight speeds, the cycloidal rotors can be slowed down and stopped, relying solely on auxiliary cruise propulsion and wing-borne lift, as can be seen in Fig. 18. The modeling of cycloidal rotor aerodynamics and wake properties is still a very much open area of investigation. There have been many publications on this topic but all focused on very small aerial vehicle (less than a few pound-force gross weight) and almost all work has been on hover performance characteristics; e.g., Refs. 32-35. The work presented in this paper relies on a novel approach using RotCFD to attempt to model cycloidal forward flight performance. And, obviously, this effort represents the first attempt to define, model, and analysis SCR aircraft. RotCFD was not modified for this SCR analysis. The cycloidal rotors were instead modeled as blades with a 90 Deg. coning angle at the prescribed hinge-offset location. Instead of conventional rotor collective being used to increase rotor thrust, blade cyclic pitch angle inputs were prescribed so that the blades would achieve their peak lift coefficients at the top and bottom rise of their rotational path. Accordingly, 'thrust' was the rms-sum of 'rotor' H-force and side force. Taking the above modeling approach was initially subject to concerns about small-angle approximations built-in to RotCFD that might reduce the accuracy of the performance estimates. This doesn't seem to be the case in the results presented in this paper. All right-hand rotors (a set of three closely aligned in a longitudinal row) spun counter-clockwise in the SCR modeling presented in this paper; all left-hand rotors were spun clockwise. There were no significant breaks (longitudinal spaces) between the set of three rotors comprising the right- or left aggregate (super-) rotors. The above assumptions regarding rotor-to-rotor spacing (within a set of rotors comprising an aggregate super-rotor) or the relative rotation direction of adjacent rotors are not cast in concrete and, of course, are subject to future aeroperformance study and design optimization. For example, a localized increase in rotor-to-rotor longitudinal separation directly underneath the aircraft's wing might allow for even greater reductions in hover download and forward fight aero interactions.

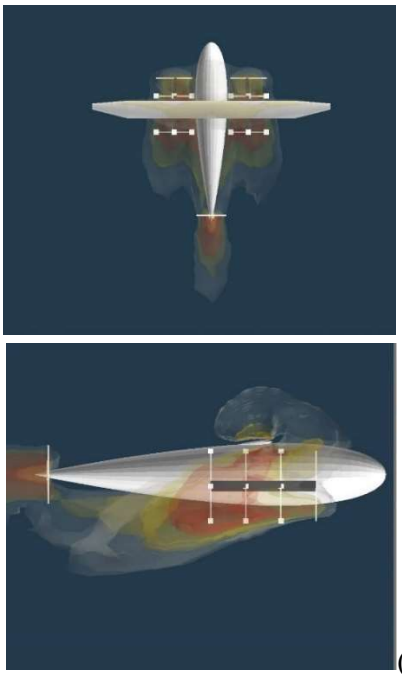

Figure 17. Transition stopped-cycloidal-rotor rotor wakes (isosurfaces of velocity magnitude); forward flight speed of 30knots (50ft/s): (a) planform and (b) side views

SCR aircraft show promise in providing a benign approach (in terms of rotor dynamics

and blade loads) to stopping rotors in midflight. Increasing forward flight behaves kinematically in the same manner and increasing wing/blade flow obliqueness (relative yaw angle sweep). As the vehicle forward flight speed increases the cycloidal rotor blades are subject to localized flow along the blade span at greater and greater effective localized yaw angles along the blade profile cross-section.

(a)

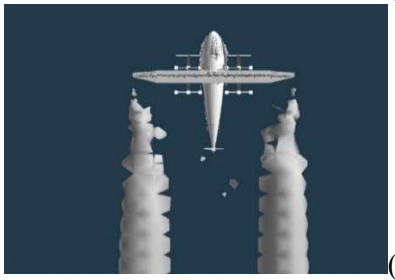

(b)

Figure 18. Top view of vehicle in high-speed flight (isosurfaces of Q-criterion): (a) V=178knots=300ft/s (half nominal hover rotor RPM) and (b) V=296knots=500ft/s (zero rotor RPM)

The cycloidal rotor hover and low-speed performance for this first generation SCR vehicle is shown below in Fig. 19.

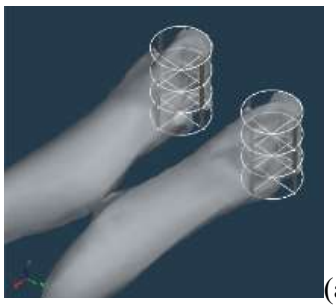

(a)

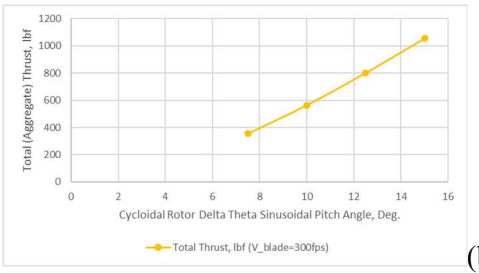

(b)

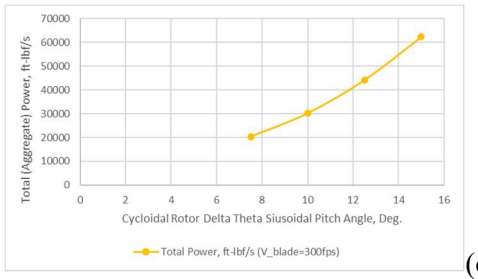

(c)

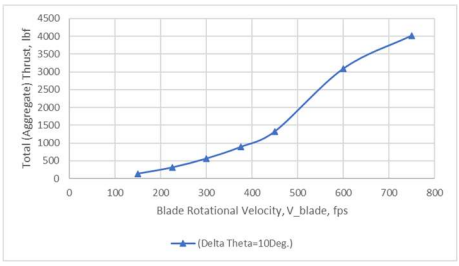

(d)

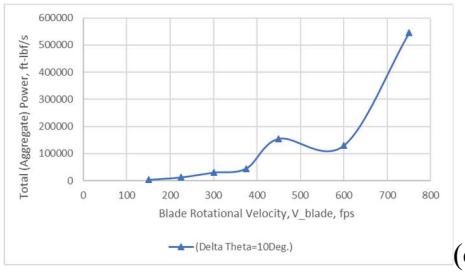

(e)

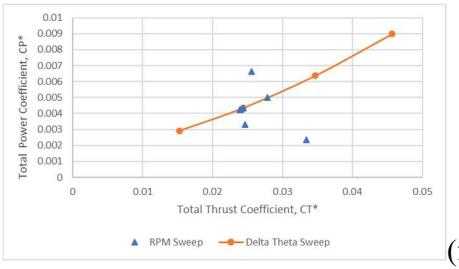

(f)

Figure 19. First generation SCR hover: (a) isolated rotor wakes; (b) Δθ and total thrust; (c) Δθ and total power; (d) V_{blade} and total thrust; (e) V_{blade} and power; (f) power and thrust polar

Figure 20 for the complete vehicle hover condition when compared with the isolated cycloidal rotor set estimates of Fig. 19 would suggest an adverse installed aerodynamic interference effect of the wing and fuselage on the rotor lift for the first generation vehicle modeled studied. Isolated rotor results would suggest a lift of 500lbf being generated, whereas Fig. 20 would suggest only 250lbf for the installed rotors.

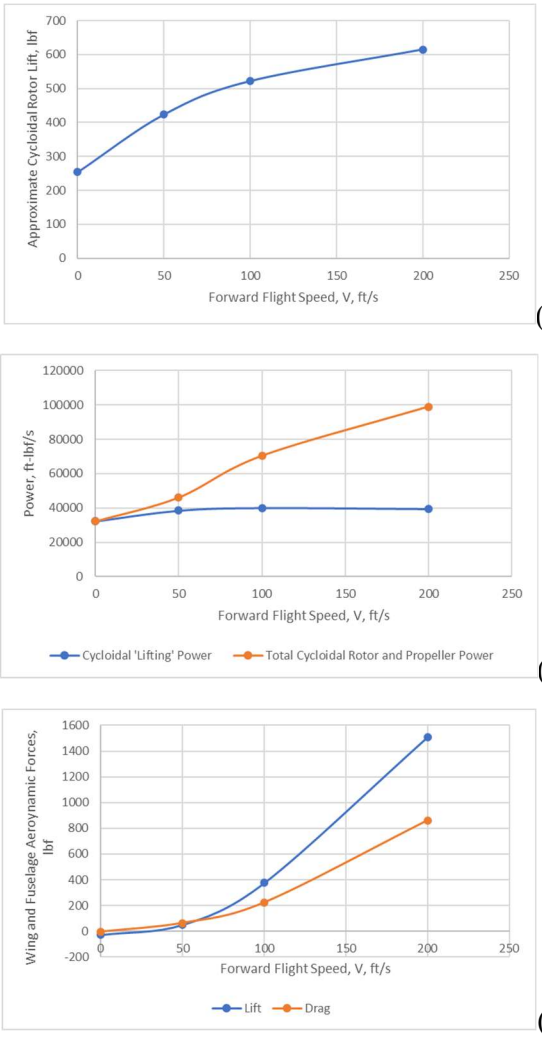

Figure 20. Forward flight rotor and airframe performance for first generation SCR (V_{blade}=300ft/s and $\Delta\theta$=10Deg.)

Figure 20c wing and fuselage lift and drag trends are the approximately parabolic trends with forward flight velocity that one would expect if there were little adverse rotors-on-wing and rotors-on-fuselage aerodynamic interference effects (this may be a consequence of the relatively light loading of the cycloidal rotors at the low V_{blade} speeds of the rotors for the results presented).

A second generation SCR vehicle (consistent with Fig. 15, i.e., a large regional aircraft) RotCFD predictions are shown in Figs. 21-23. The cycloidal rotor wakes shown as velocity magnitude isosurfaces are generally consistent with the first generation UAV or small-aircraft configuration results shown in Figs. 16-20. The cycloidal rotor wakes are approximately rectilinear and skew backwards as forward flight velocities are increased. Once the vehicle is taken to the transition/conversion speed, the rotors are slowed down and stopped. Which, for the cycloidal rotor geometry studied in this paper, this transition/conversion is relatively benign as far as adverse aerodynamic loads on the rotors/rotor-blades are concerned.

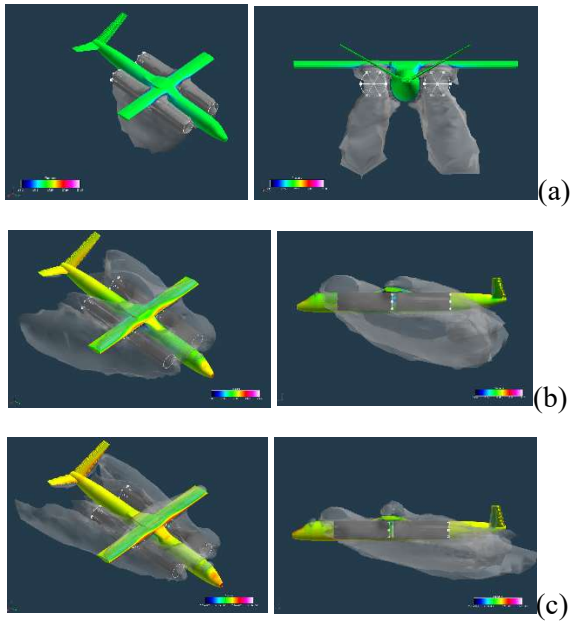

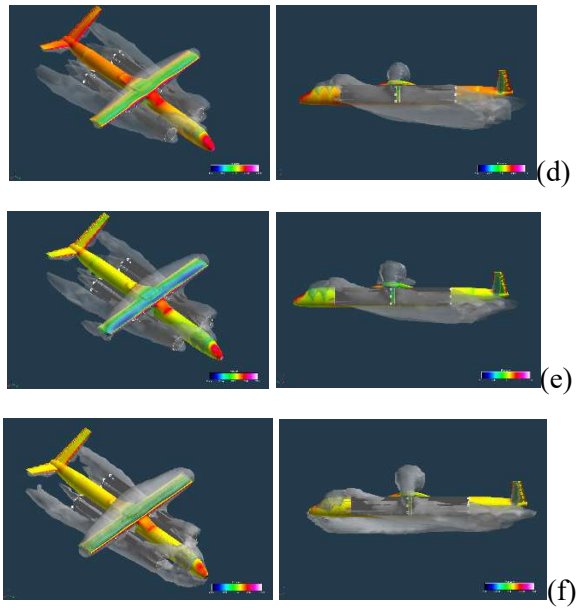

Figure 21. Second generation SCR Vehicle surface pressures and rotor wakes: (a) hover, (b) low speed 30knots (50ft/s) forward flight, (c) 59knots (100ft/s), (d) 89knots (150ft/s), (e) 118knots (200ft/s), and (f) 148knots (250ft/s)

Figure 22a-f presents some of the hover performance trends of the second generation SCR vehicle (as compared to Fig. 19a-f for the first generation vehicle). Note that equivalent blade rotational speeds (V_{blade}=750 ft/s) and delta pitch angle inputs ($\Delta\theta$=10 Deg.) for the two generations of vehicles, with their corresponding different missions (i.e., UAV or small-aircraft versus regional passenger-carrying vehicle) yields respectively ~4500 lbf versus ~100,000 lbf of lift generation in hover for the two different aircraft. Note, some of power estimate scatter observed for the first generation SCR isolated rotors are not observed in the second generation SCR cycloidal rotor hover performance results; this remains an opportunity for future study.

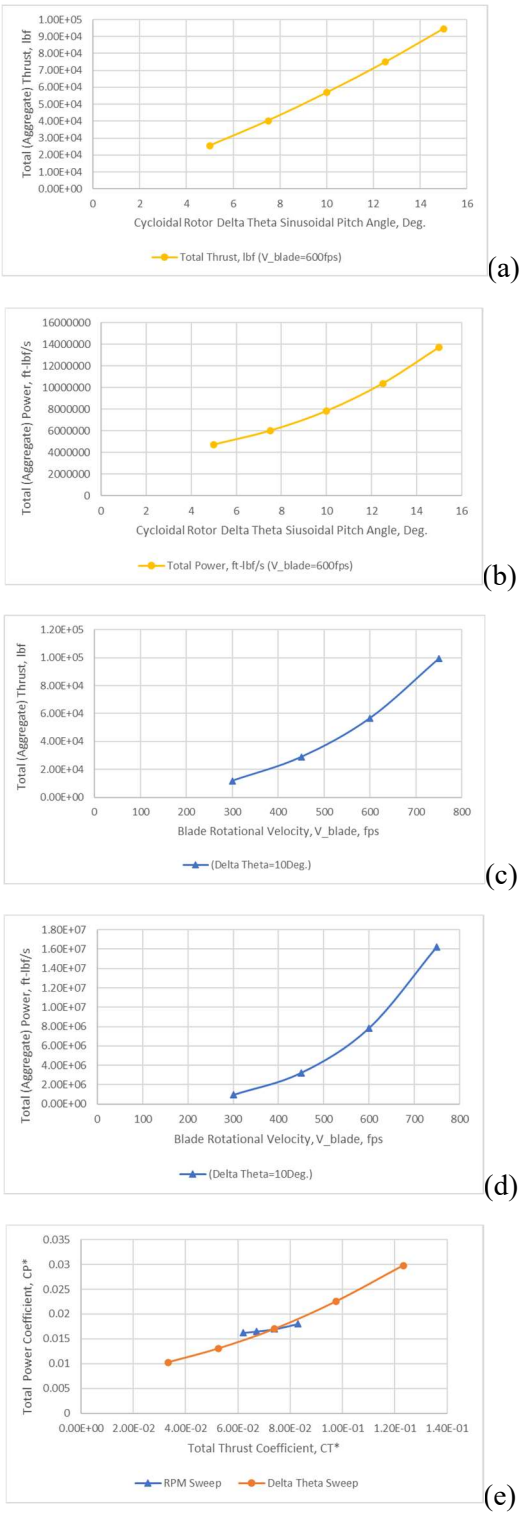

Figure 22. Second generation SCR hover performance trends: (a) sinusoidal $\Delta\theta$ inputs on total thrust; (b) $\Delta\theta$ on total power; (c) V_{blade} on total thrust; (d) V_{blade} on power; and (e) power and thrust coefficient polar

Figure 23 illustrate the rotor lift and power trends with hover and forward flight prior to transition/conversion to stopped-rotor operation.

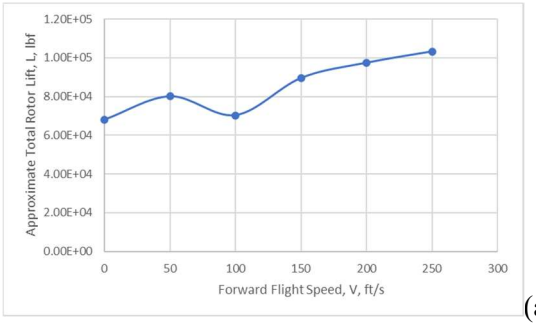

(a)

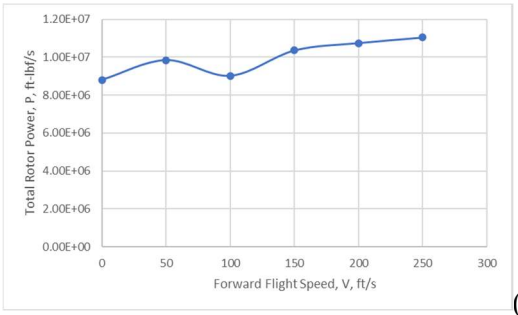

(b)

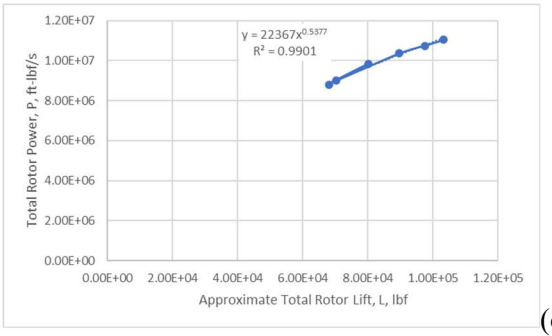

(c)

Figure 23. Second generation SCR cycloidal rotor performance for hover, low-speed, and near-transition/conversion to stopped-rotors: (a) rotor total (approximate) lift as a function of forward flight speed; (b) rotor total power as a function of forward flight speed; (c) rotor total power as a function of rotor total (approximate) lift

Figure 24 illustrates the aerodynamic interactions of the cycloidal rotors on the combined wing and fuselage lift and drag.

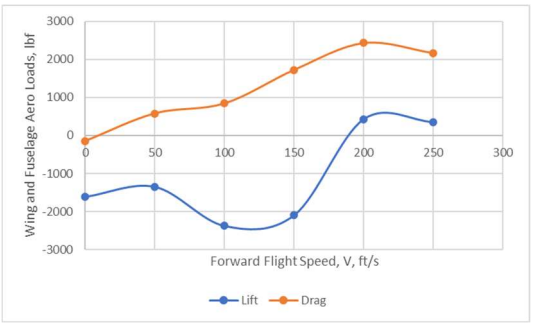

Figure 24. Aerodynamic interactions of cycloidal rotor on vehicle airframe (zero angle-of-attack)

The approach taken for SCR sizing when it comes to the cycloidal rotor performance in hover and pre-conversion/pre-stopped-rotor flight was earlier discussed in the paper as to the use of rotor surrogate models. The following comments now discuss the weight estimation methodology used for SCR sizing employed in this paper. First, for all four vehicle configurations studied in this paper, there is a generation assumption that wing weight decreases (from a conventional baseline ~300knot tractor-proprotor tiltrotor aircraft) because of the use of thinner wings to have efficient (lower compressibility drag) flight at speeds greater than 400knots. As a minimum, for the second generation mission and aircraft it is assumed that ~21-24% thick wing of a conventional tiltrotor aircraft will be replaced with an ~18% thick wing (this could result in a 18/24, or ~25%, reduction in wing weight with thickness reduction). (Note that this reduction in wing thickness may not be incorporated in wing weight estimates for the first generation aircraft, because of their lower cruise speeds and altitude.) This wing weight reduction, though, might be negated if higher aspect ratio wings are used for the 400knot plus aircraft versus a 300knot baseline; such an increase in wing aspect ratio probably makes most sense for the SCR aircraft as compared to the other three

concepts. Cruise L/D efficiency (and whirl-flutter stability for wing-mounted rotors) does not necessarily size wing thickness; instead, wing thickness and stiffness may be sized by 'jump' loads during takeoff. Second, the rotor design for an SCR aircraft is significantly different as compared to a conventional helicopter/tiltrotor rotor; accordingly, it is simplistically assumed the rotor weight is 5% of gross weight. Third, the control systems and drive systems for a SCR aircraft will also be quite different from conventional rotorcraft, which, in turn, means that the weight estimation methodology will be quite different. Without detailed mechanical design of such unique systems, an correction factor to the fuselage weight (5% increase to be assumed) to globally account for the weight increases of SCR aircraft over analogous subsystem weights for conventional rotorcraft.

Table 8. First-order vehicle sizing for first generation (UAV/small-aircraft) SCR aircraft concept

Stopped Cycloidal Rotor Blade Span	3.00	ft
Cycloidal Rotor Blade Radial Offset from Rotation Axis	3.00	ft
Number of Blades	4.00	Nondim.
Total Rotating Blade Area	43.77	ft^2
Cycloidal Rotor Blade (Uniform) Rotational Speed	598.03	ft/s
Nominal (Mean) Airplane-Mode Cruise Wing Loading	107.86	lbf/ft^2
Wing Span	7.79	ft
Number of Electric Motors per Rotor	1.00	Nondim.
Hover Power	108.78	Hp
Advance Ratio	0.21	Nondim.
Nominal Helicopter-Mode Forward Flight Power	459.75	Hp
Vehicle Effective Lift over Drag in Airplane-Mode Cruise	12.00	Nondim.
Nominal (Mean) Airplane-Mode Cruise Power	263.83	Hp
Energy from Battery over Total Mission Energy	0.13	Nondim.
Prescribed Fraction of Power Delivered by Electric Motors in Hover versus Turboshaft Engines	0.25	Nondim.
Prescribed Fraction of Power Delivered by Electric Motors in Helicopter-Mode Forward Flight versus Turboshaft Engines	0.25	Nondim.
Prescribed Fraction of Power Delivered by Electric Motors in Airplane-Mode Cruise versus Turboshaft Engines	0.00	Nondim.
Payload (an/or Combined Passenger(s) and Crew)	500.00	lbf
Total Weight of Rotors	94.48	lbf
Fuselage Weight	15.92	lbf
Wing Weight	1098.12	lbf
Total Convertible Engines and Drive Train Weight	659.26	lbf
Total Fuel Weight	60.65	lbf
Total Battery Weight	75.39	lbf
Total Electric Motor Weight	35.18	lbf
Total Fixed Equipment Weight	100.15	lbf
Total TOGW =	2639.15	lbf

Table 9. First-order vehicle sizing for second generation (large, passenger-carrying regional) SCR aircraft concept

Stopped Cycloidal Rotor Blade Span	28.00	ft
Cycloidal Rotor Blade Radial Offset from Rotation Axis	4.00	ft
Number of Blades	6.00	Nondim.
Total Rotating Blade Area	2178.90	ft^2
Cycloidal Rotor Blade (Uniform) Rotational Speed	598.03	ft/s
Nominal (Mean) Airplane-Mode Cruise Wing Loading	99.19	lbf/ft^2
Wing Span	10.76	ft
Number of Electric Motors per Rotor	1.00	Nondim.
Hover Power	20904.13	Hp
Advance Ratio	0.21	Nondim.
Nominal Helicopter-Mode Forward Flight Power	35759.82	Hp
Vehicle Effective Lift over Drag in Airplane-Mode Cruise	12.00	Nondim.
Nominal (Mean) Airplane-Mode Cruise Power	14071.12	Hp
Energy from Battery over Total Mission Energy	0.13	Nondim.
Prescribed Fraction of Power Delivered by Electric Motors in Hover versus Turboshaft Engines	0.25	Nondim.
Prescribed Fraction of Power Delivered by Electric Motors in Helicopter-Mode Forward Flight versus Turboshaft Engines	0.25	Nondim.
Prescribed Fraction of Power Delivered by Electric Motors in Airplane-Mode Cruise versus Turboshaft Engines	0.00	Nondim.
Payload (an/or Combined Passenger(s) and Crew)	12500.00	lbf
Total Weight of Rotors	5902.59	lbf
Fuselage Weight	21250.10	lbf
Wing Weight	6739.72	lbf
Total Convertible Engines and Drive Train Weight	17992.00	lbf
Total Fuel Weight	13473.14	lbf
Total Battery Weight	16873.02	lbf
Total Electric Motor Weight	3830.31	lbf
Total Fixed Equipment Weight	6951.94	lbf
Total TOGW =	105512.83	lbf

By way of comparison, two alternate (novel or little explored) high-speed rotorcraft configurations will also be discussed to a modest degree. A brief summary of the two alternate (non-stopped-rotor) high-speed rotorcraft is presented immediately below.

NOVEL NON-STOPPED-ROTOR HIGH-SPEED ROTORCRAFT

Two non-stopped-rotor (alternate) high-speed rotorcraft concepts will now be briefly discussed. Stopped-rotor aerial vehicles are hardly the only notional means by which high-speed (greater than 400 knots), high-hover-efficiency VTOL flight could be achievable.

Pusher-Proprotor Tiltrotor Aircraft

The pusher-proprotor tiltrotor (PPT) aircraft is an 'old' VTOL aircraft design concept dating all the way to the 1940's. Despite that long heritage it has largely gone

unexplored in terms of rotorcraft research. It was suggested, Ref. 11, that this vehicle concept be reexamined in the context of being a potential high-speed rotorcraft configuration.

A pusher-type tiltrotor configuration might have performance and weight benefits over the conventional tractor-type proprotor design. This paper focuses on vehicle sizing studies using a simple spreadsheet-type rotorcraft sizing analysis. This simple sizing analysis has been previously used in Ref. 13, for example. Additionally, this paper will examine vehicle aerodynamics, especially wing-on-rotor aerodynamic interaction effects, in cruise. This complements some of the work related to wing-on-rotor and rotor-on-wing aerodynamic interactions in hover presented earlier in Ref. 11.

Table 10 is a partial list of the pros, cons, known unknowns, and technical challenges of pusher-proprotor tiltrotor (PPT) aircraft.

Table 10. Pros, cons, known unknowns, and technical challenges for Pusher-Proprotor Tiltrotor aircraft concept

Pros:
1. Reduces wing download in hover as compared to conventional tractor-type proprotors (refer to Ref. 11 for initial analysis of this aero benefit)
2. Perhaps the lightest weight vehicle option for high-speed rotorcraft missions (if the rotor/wing whirl flutter problem can be addressed by use of pusher proprotors); lighter and more efficient (at high cruise speeds) wings could potentially be used instead of the relatively thick wings (~21-24%) used for conventional tiltrotor aircraft. Additionally, auxiliary propulsion systems (with or without the use of convertible engines) would not need to be employed; instead, all propulsive force would still come from the pusher proprotors for all phases of flight
Cons:
1. Landing gear design will be a challenge because of the low ground clearance issues; long, stiff multi-degree-of-freedom articulated legs might be one solution; alternatively, use of a static mast through the center of the rotating rotor shafts (and hubs) might allow an attachment of 'rotor mast mounted' landing gear
2. This vehicle configuration might not be suitable for military missions, only civilian/commercial, because of the low ground clearance of the pusher-proprotors
Known Unknowns:
1. Implications of hover performance and control in very close proximity to the ground; some past work in the literature suggests that there is a drop-off of rotor thrust for rotor heights h/R<1, e.g., Ref. 36. This, though, is an open question for future study
2. Still an open question of whether a pusher proprotor has, in general, better whirl flutter characteristics than conventional tractor-type proprotor tiltrotor aircraft
Technical Challenges:
1. Computational and small-scale experimental evaluation of whirl flutter characteristics of pusher-proprotor tiltrotor aircraft
2. Consideration of downstream wing wake effects on rotor mean and distributed aero loads and overall performance; optimal rotor spacing with respect to vehicle wing would need to be further studied to minimize adverse effects of such wing aero interactions in forward flight

The goal of such pusher-proprotor tiltrotor research is to potentially enable the development of small autonomous aerial vehicles of this type and, perhaps even more ambitiously, larger aircraft to meet the future transportation needs of the traveling public. However, there are challenges in developing such aircraft. Ground clearance issues would be very important for transport aircraft with pusher-proprotors; passengers and cargo would be loaded from the rear of the aircraft by means of a ramp. Because of the unique nature of a pusher-proprotor configuration, turbine engine mounting cannot be wing-tip mounted (coincident with the rotor nacelles) as is conventional tractor-type tiltrotor aircraft. Turbine exhaust gas temperatures would be much too high to run the risk of their ingestion into the rotor disk plane – and thus run the chance of damaging the rotor hardware. Therefore, pusher-proprotor tiltrotor aircraft will have to have the turbine engines fixed-mounted horizontally at the wing and fuselage junction, or, alternatively, on the empennage/tail of the aircraft. Either location will require some creative drivetrain designs to allow for lightweight but robust interconnect shafting between the engines and the rotor nacelles.

The conversion process is seen in Fig. 25a-d below; this ranges from hover and low-speed helicopter-mode (with the PPT rotors suspended below the wing as inherent in the design concept), early and late stages of transition/conversion, followed by cruise. (No rotor nacelles are shown in Fig. 25a-d for simplicity.) It can be clearly seen in rotor disk differential pressures in some of the Fig. 25a-d results that the wing induced flow field in forward flight can have a noticeable influence on the rotor disk loading distribution. This is a unique aerodynamic challenge for PPT versus conventional tractor-type proprotor tiltrotor aircraft (which sees more of an influence in hover on disk loading distribution than during forward flight). In hover, both PPT and tractor-type proprotors wakes results in download forces on the wings and the fuselage of the aircraft; these download forces, however, are generally lower for PPT.

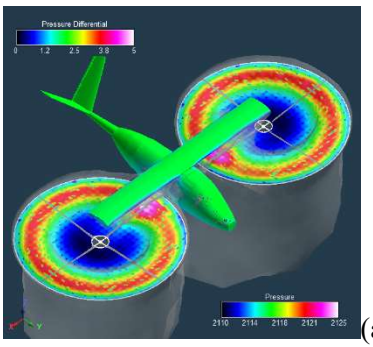

(a)

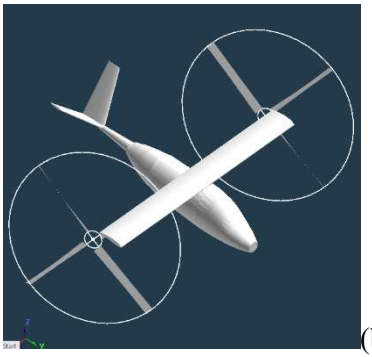
(b)

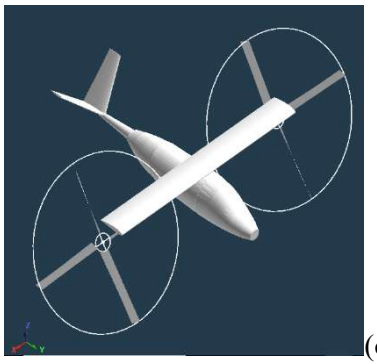
(c)

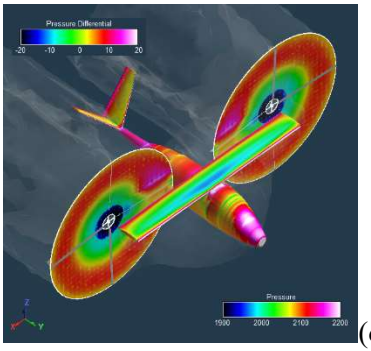
(d)

Figure 25. First generation PPT Aircraft: (a) helicopter-mode hover; (b) transition forward flight, i_N=60 Deg., V=118knots=200ft/s, AOA=0 Deg.; (c) i_N=30 Deg., V=148knots=250ft/s, AOA=0 Deg.; (d) cruise forward flight, i_N=90 Deg., V=250knots=422ft/s, AOA=0 Deg.

Figure 26a-c illustrates an angle-of-attack sweep of the first generation PPT vehicle. It presents color contour of the rotor differential pressures across the rotor disks, as well as surface pressure contours and rotor wake velocity magnitude isosurfaces.

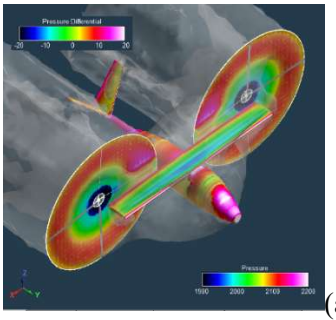
(a)

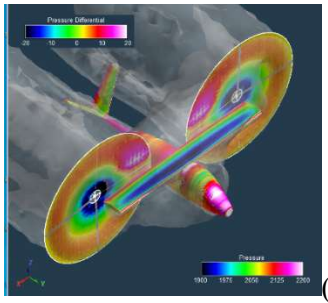
(b)

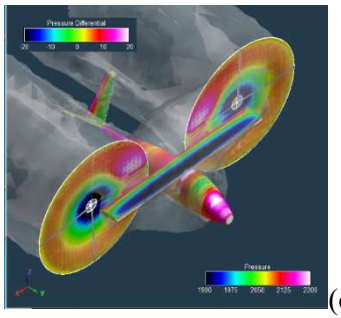
(c)

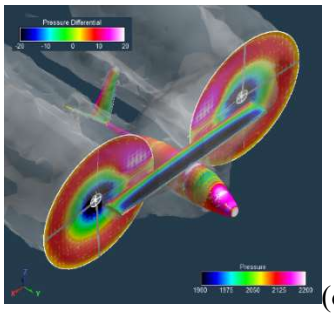
(d)

Figure 26. First generation PPT cruise angle-of-attack sweep: (a) AOA=0Deg., (b) AOA=2Deg., (c) AOA=4Deg., and (d) AOA=6Deg.

As can be seen from the rotor differential pressures across the PPT rotor disks in Fig. 26a-d, the wing induced velocity field downstream of the wing and upstream of the pusher-proprotors does have a nonnegligible impact of the rotor differential pressure distributions. And, as shown in Fig. 27, the wing induced velocity flow field entrained into the pusher-proprotors also has an impact on the mean thrust and other forces of the rotors as well.

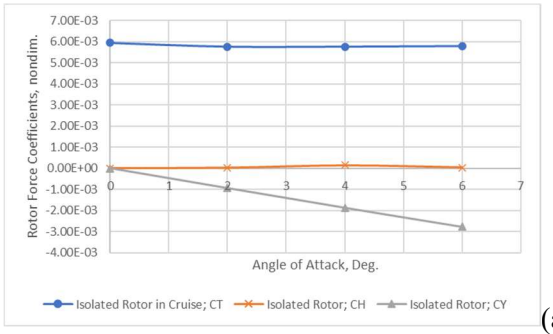

(a)

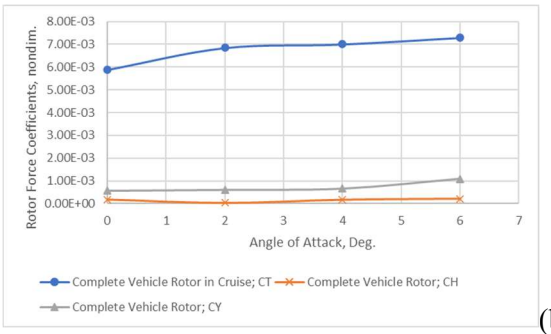

(b)

Figure 27. Impact on rotor force coefficients for PPT as a function of angle of attack: (a) isolated rotor in cruise (V=250knots=422ft/s) and (b) rotor as affected by aero interactions in cruise

Modest values of L/D are predicted for the notional vehicle design model used in the RotCFD predictions of the first generation PPT aircraft; refer to Fig. 28. These modest L/D values are consistent, for example, with a comparable sized test model (a quarter-scale V-22) documented in Ref. 9. Higher L/D values for the LCTR2 geometry (which was used as the baseline fuselage and wing geometry used for the second generation vehicles studied in this paper) have been established both computationally as well as experimentally, e.g., Ref. 45. The first generation SCR wing is constant chord with aspect ratio is AR=8 and the total wing planform area is S=200 ft^2. This wing geometry was selected prior to the sizing analysis presented latter in this paper.

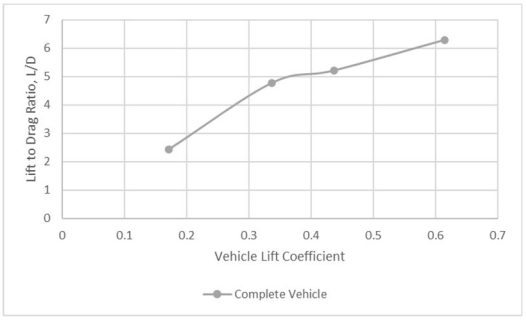

Figure 28. Complete first generation PPT vehicle lift-to-drag ratio, L/D

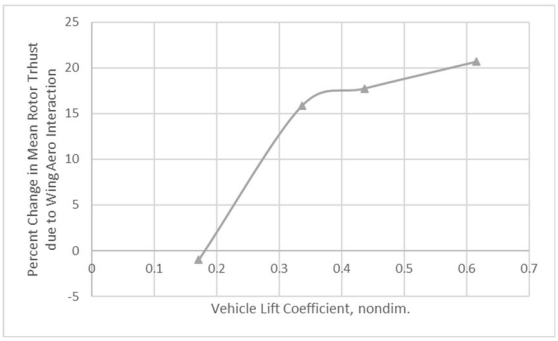

Figure 29. Impact of wing lift coefficient (because of AOA sweep) on mean rotor thrust coefficient in cruise for pusher-proprotors

The net effect of PPT rotor installation is that the installed mean rotor power is increased by 3 to 9% over isolated rotor power during cruise. This can be clearly seen in Fig. 30.

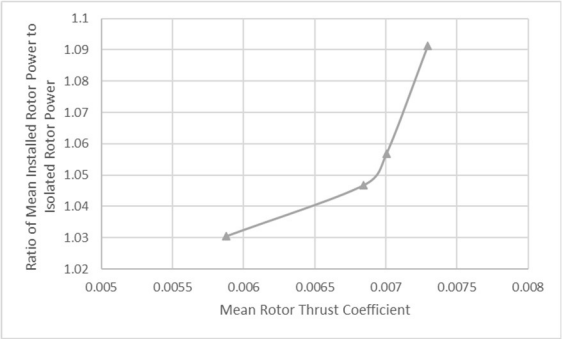

Figure 30. Ratio of installed cruise (V=422 ft/s) PPT mean rotor power coefficient over isolated rotor power coefficient as a function of installed thrust coefficient

Figure 31a-c illustrates the hover, transition, and cruise phases of flight for the second generation PPT aircraft; rotor wake velocity magnitude isosurfaces and rotor disk differential pressures are also shown.

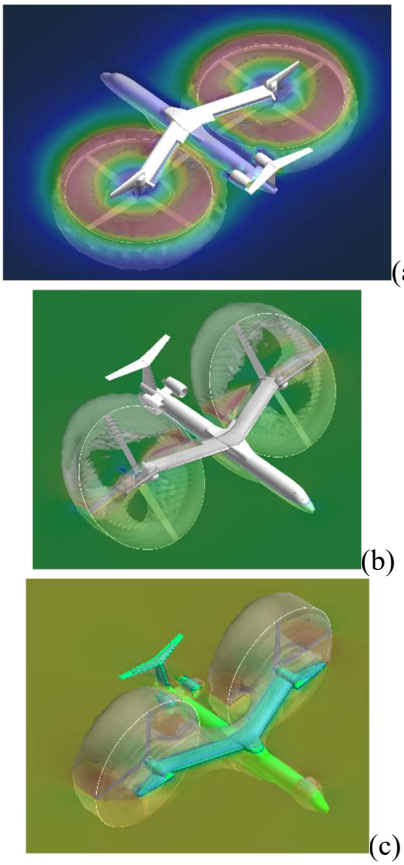

Figure 31. Second generation PPT aircraft flow fields: (a) hover, (b) transition, and (c) cruise forward flight

In performing PPT aircraft sizing analysis, simple hover and cruise aerodynamic interference factors are used. The wing-on-rotor aerodynamic interference effects in hover for a PPT aircraft are smaller than that of a conventional baseline (tractor-proprotor with cruise speeds under 300knots). However, those wing-on-rotor aerodynamic interference effects for PPT aircraft are greater in cruise (because the proprotors are downstream of the wing wake) than for conventional tiltrotor aircraft (in which case the rotors are upstream of the wing). Correspondingly, rotor-on-wing (download) aero interference effects for conventional tiltrotor aircraft are larger than that for PPT aircraft (PPT have less hover download than conventional tiltrotors). The same is true in cruise, the rotor-on-wing aero interferences are greater from conventional tiltrotors as compared to PPT. For the purposes of the PPT sizing analysis performed in this paper, the wing-on-rotor and rotor-on-wing aero interference effects are predicted to first order confidence using the RotCFD software tool and then incorporated into the spreadsheet-style sizing analysis. The weight estimation approach for PPT aircraft as used for this paper is now discussed. First, most system/subsystem weight estimates for a PPT aircraft can make use of the same estimation methodology for conventional tiltrotor aircraft. Second, to start discussing estimation differences between PPT and conventional tiltrotor aircraft, the foremost biggest differences lie with: (1) increased drive train and gearbox complexity and weight to mount turboshaft engines on the fuselage and then route drive shafts and coupling from the engines to the wing-mounted nacelles (wing-mounted engines as in XV-15, AW609, and V-22 tiltrotors would not be acceptable for PPT aircraft as engine exhaust into or near the pusher-proprotors would likely not be acceptable from a heat-damage perspective); a weight increase of 25% is assumed for a PPT aircraft versus a conventional tractor-proprotor tiltrotor with wing-mounted engines; (2) potential increased weight due to longer and more robust landing gear/legs (for rotor clearance near the ground when taking off or landing); a 5% increase in fuselage weight is assumed for the increased landing gear weight; (3) PPT aircraft wings are swept back, not forward like conventional tiltrotor aircraft; this, though, is assumed to have a neutral effect on overall wing weight; (4) small increases in control system weight and rotor weight are anticipated to reflect going to

400knots (versus ~300knots); a 5% increase is used in the sizing analysis; (5) small to modest decreases are anticipated for wing weight to reflect going to a thinner wing (18% versus ~21-24% thick) more consistent with higher cruise speed; a 10% weight reduction in wing weight is assumed for being able to go to a thinner wing.

A hover download of 2% is used in the analysis, as compared to the 7-10% download for conventional tractor-proprotor tiltrotor aircraft. A six-percent cruise power increase (over that of an isolated rotor power estimate) is used to account for the installed rotor power of a PPT aircraft (based on the predicted results of Fig. 31).

A coarse weight iteration convergence tolerance (<0.75%) is used in the sizing analysis results.

Table 11. First-order vehicle sizing for first generation (UAV/small-aircraft) pusher-proprotor tiltrotor (PPT) aircraft concept

Main Rotor Disk Loading	20.32	lbf/ft^2
Main Rotor Radius	4.97	ft
Number of Blades	4.00	Nondim.
Main Rotor Solidity	0.12	Nondim.
Main Rotor Tip Speed	781.53	ft/s
Nominal (Mean) Airplane-Mode Cruise Wing Loading	107.83	lbf/ft^2
Wing Span	12.89	ft
Number of Electric Motors per Rotor	1.00	Nondim.
Hover Power	272.89	Hp
Advance Ratio	0.21	Nondim.
Nominal Helicopter-Mode Forward Flight Power	127.57	Hp
Vehicle Effective Lift over Drag in Airplane-Mode Cruise	6.00	Nondim.
Nominal (Mean) Airplane-Mode Cruise Power	652.55	Hp
Energy from Battery over Total Mission Energy	0.07	Nondim.
Prescribed Fraction of Power Delivered by Electric Motors in Hover versus Turboshaft Engines	0.25	Nondim.
Prescribed Fraction of Power Delivered by Electric Motors in Helicopter-Mode Forward Flight versus Turboshaft Engines	0.25	Nondim.
Prescribed Fraction of Power Delivered by Electric Motors in Airplane-Mode Cruise versus Turboshaft Engines	0.00	Nondim.
Payload (and/or Combined Passenger(s) and Crew)	500.00	lbf
Total Weight of Rotors	20.93	lbf
Fuselage Weight	22.51	lbf
Wing Weight	1487.94	lbf
Total Turboshaft Engines and Drive Train Weight	154.70	lbf
Total Fuel Weight	97.33	lbf
Total Battery Weight	334.10	lbf
Total Electric Motor Weight	134.47	lbf
Total Fixed Equipment Weight	326.48	lbf
Total TOGW =	3078.45	lbf

Table 12. First-order vehicle sizing for second generation (large, passenger-carrying regional) pusher-proprotor tiltrotor (PPT) aircraft concept

Main Rotor Disk Loading	20.32	lbf/ft^2
Main Rotor Radius	24.47	ft
Number of Blades	4.00	Nondim.
Main Rotor Solidity	0.12	Nondim.
Main Rotor Tip Speed	781.53	ft/s
Nominal (Mean) Airplane-Mode Cruise Wing Loading	101.79	lbf/ft^2
Wing Span	65.15	ft
Number of Electric Motors per Rotor	1.00	Nondim.
Hover Power	5798.82	Hp
Advance Ratio	0.21	Nondim.
Nominal Helicopter-Mode Forward Flight Power	2355.29	Hp
Vehicle Effective Lift over Drag in Airplane-Mode Cruise	12.00	Nondim.
Nominal (Mean) Airplane-Mode Cruise Power	10565.07	Hp
Energy from Battery over Total Mission Energy	0.06	Nondim.
Prescribed Fraction of Power Delivered by Electric Motors in Hover versus Turboshaft Engines	0.25	Nondim.
Prescribed Fraction of Power Delivered by Electric Motors in Helicopter-Mode Forward Flight versus Turboshaft Engines	0.25	Nondim.
Prescribed Fraction of Power Delivered by Electric Motors in Airplane-Mode Cruise versus Turboshaft Engines	0.00	Nondim.
Payload (an/or Combined Passenger(s) and Crew)	12500.00	lbf
Total Weight of Rotors	7355.37	lbf
Fuselage Weight	12367.19	lbf
Wing Weight	7784.60	lbf
Total Turboshaft Engines and Drive Train Weight	14001.44	lbf
Total Fuel Weight	5846.42	lbf
Total Battery Weight	7574.26	lbf
Total Electric Motor Weight	2103.01	lbf
Total Fixed Equipment Weight	4847.98	lbf
Total TOGW =	74380.28	lbf

Noncircular-Duct Tilting/Pivoting Ducted Fan Aircraft

The concept of two-degree-of-freedom (2DOF) tilting and pivoting nacelles (2DOF-TP) was first introduced in Ref. 11 for tiltrotor aircraft. The utility of 2DOF pivoting and tilting mechanisms for ducted-fan vehicles also has similar promise; refer to Fig. 32.

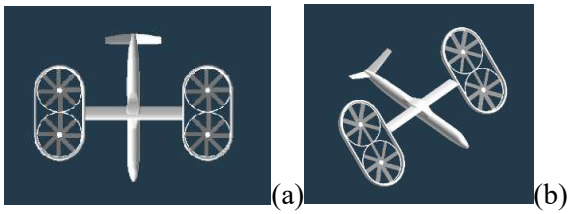
(a) (b)

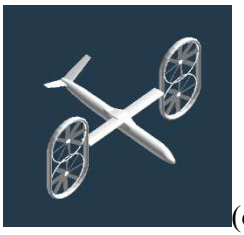
(c)

(d)

Figure 32. Views of second generation (regional passenger-carrying) 2DOF-TP vehicle: i_N=0 and i_P=0; (b) i_N=45 and i_P=0; (c) i_N=90 and i_P=0; (d) i_N=90 and i_P=75

Ducted-fan vehicles have been studied extensively; during the 2000-2015 timeframe most of the research has been focused on small vehicles or UAVs, e.g., Refs. 37-38. Recently ducted-fan vehicles (both tilting- and non-tilting-nacelle types) have regained interest with respect to urban air mobility (UAM) missions. Additionally, sizing work for UAM tiltrotor and ducted-fan aircraft has been performed through use of well-known NASA conceptual design NDARC; Refs. 39-40.

Table 13 is a partial list of pros, cons, known unknowns, and technical challenges for 2DOF tilting and pivoting ducted fan aerial vehicles.

Table 13. Pros, cons, known unknowns, and technical challenges for 2DOF pivoting and tilting ducted fan aircraft concept

Pros:
1. Tilting ducted-fan aircraft have added protection for passengers and the community as the rotors/fans are embedded in protective shrouds (i.e., the ducts)
2. Oval ducts (1- or 2-DOF) with embedded tandem-fan arrangements provide for simple rpm/collective-based flight control in hover and low-speed flight (refer to Ref. 13)
3. Ducted fans can provide hover 'thrust augmentation' above that of just the fan thrust alone; ducts can provide lift augmentation during transition/tilting from helicopter-mode operation to airplane-mode
4. Adding the second degree-of-freedom to the ducts by pivoting them, after tilting, potentially could result in increased cruise L/D
5. Higher disk loading fans could/should be used for ducted-fan vehicles; there are some positive aspects of using higher disk loading fans than otherwise used for open-rotor/fan configurations (there are also well-recognized drawbacks), including increased noise (though arguably ducts could help attenuate the noise from the stronger acoustic sources) and increased rotor outwash velocities
6. Auxiliary propulsion systems might not be required for ducted-fan high-speed rotorcraft; that additionally implies that convertible engines may not be required; higher disk loading ducted-fans might require small compact high-power/higher-torque motors than equivalent lower rotor disk loading high-speed rotorcraft concepts and, thereby, might represent a technology 'push' beyond current development efforts
Cons:
1. A 2DOF tilting/pivoting nacelle/ducted-fan vehicle seems to be relatively new concept (see Ref. 11 for discussion regarding 2DOF tilt/pivot proprotors/nacelles for "tiltrotor" aircraft)
2. Ducts can have very high drag and pitching moments during tilting; there is a tradeoff between thicker duct airfoils for hover thrust augmentation versus low profile drag during transition and high-speed flight
3. The large oval ducts will likely need distributed flaperons on their side panels to aid in overall vehicle static trim control during tilting and pivoting, because of the extremely large shifts in center of mass and center of lift/pressure of the vehicle during tilting and pivoting
4. Ducts (and their associated support struts and control vanes) are very heavy and could have high drag; it is not clear that the benefits during hover and low-speed flight justify their (the ducts) use given the potential downsides of their use during transition and cruise
Known Unknowns:

1. What are the tradeoffs between smaller, higher disk loading fans – and, therefore, small ducts – for good aeroperformance and static trim control during transition/cruise versus large fans/ducts for providing improved simpler pitching moment flight control during hover and low-speed flight; some sort of optimal vehicle design analysis needs to be developed to consider this problem
2. How much vane control in the interior of the ducts and flaperons on the outer side panels of the ducts need to be included in the vehicle designs for good vehicle static trim flight control for all phases of flight
Technical Challenges:
1. Reducing duct wetted area while still providing good hover thrust augmentation characteristics
2. Duct shaping, wing/duct integration, and the value of pivoting vs. just tilting for cruise L/D

Figure 33 illustrates one conceptual design implementation; the objective of the 2DOF tilting mechanism to transform the rectangular side panels of oval ducts to horizontal lifting surfaces during high-speed cruise flight. Accordingly, such 2DOF tilt-nacelle, ducted fan vehicles might have performance advantages over more conventional 1DOF tilting circular-ducted fan vehicles. On the other hand, robust mechanical design of the tilting mechanism would be no doubt challenging. And, further, static fixed-wing surface trim control would place novel demands on the tail/elevator design for such VTOL aircraft. Finally, the side panels of the oval ducts might also require flaperons during the tilt/pivot transition.

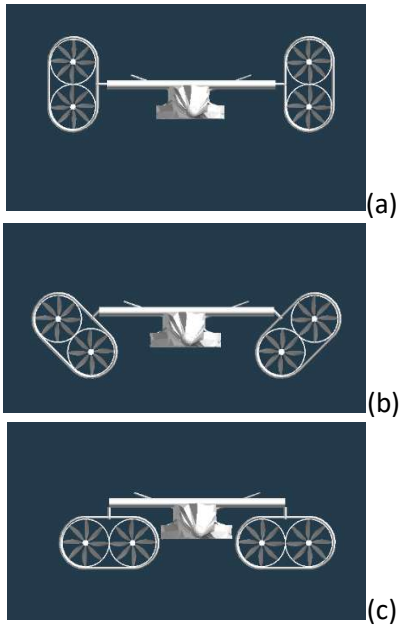

Figure 33. One possible (first generation model geometry) 2DOF-TP Vehicle: (after ducts tilted to i_N = 90Deg.): (a) pivot at 0Deg., (b) pivot to 45Deg., and (c) pivot to 90Deg.

Some RotCFD predictions are shown in Figs. 34-37 for the Fig. 26 first generation vehicle configuration (a UAV or small aircraft). The RotCFD work encompasses the flight regimes of 2DOF pivoting/tilting vehicle through hover, transition (tilting), transition (pivoting), and cruise. The hover and low speed flight (pre-pivot transition) are reproduced from the work of Ref. 13.

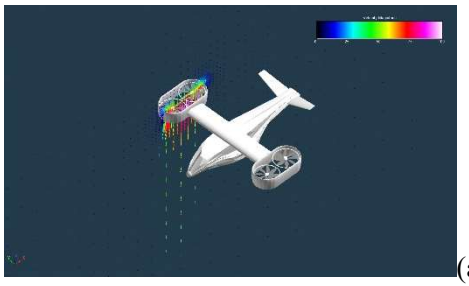

(a)

(b)

(c)

Figure 34. Hover and low-speed first generation (consistent with a UAV or small aircraft) 2DOF tilting/pivoting ducted fan aerial vehicle and rotor wakes: (a) hover, i_N=90 Deg.; (b) in the middle of tilt transition, 150 ft/s, i_N=60 Deg.; (c) near the end of tilt transition, 200 ft/s, i_N=30Deg.

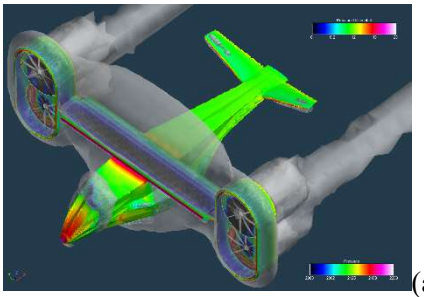

(a)

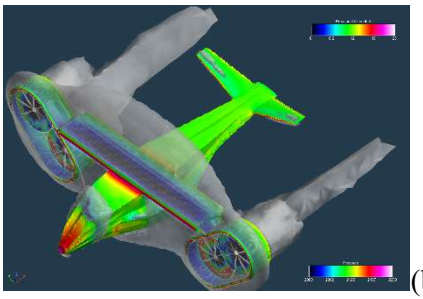

(b)

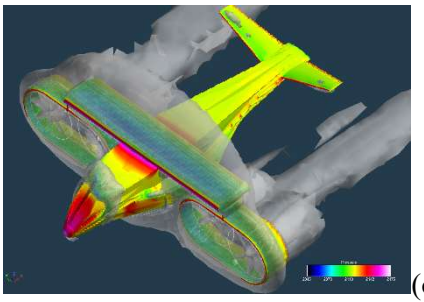

(c)

Figure 35. Mid- to late-transition first generation (UAV or a small-aircraft) 2DOF pivoting/tilting ducted fan aerial vehicle and rotor wakes: (a) beginning of pivot transition, i_N=0 Deg. and i_P= 0 Deg.; (b) middle of pivot transition, i_N=0 Deg. and i_P= 45 Deg.; (c) end of pivot transition, cruise configuration, i_N=0 Deg. and i_P= 90 Deg.

Lift and drag characteristics of the first generation 2DOF-TP vehicle are presented in Fig. 36. Partial lift and drag breakdowns are also presented, wherein the fuselage only without the v-tail, the fuselage with the v-tail, and the fuselage and wing lift and drag trends with angle of attack are shown.

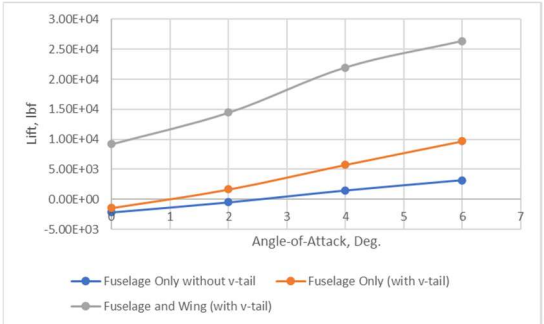

(a)

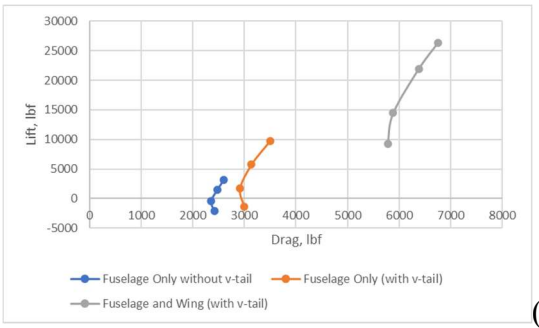

(b)

Figure 36. Fuselage, and fuselage and wing, lift and drag trends with angle of attack (without tilting/pivoting oval ducts and fans)

The inclusion of the oval ducted fans roughly triples the total wing/duct wetted area of vehicle (as compared to just the wing wetted area alone). Figure 37 presents the complete vehicle lift, drag, and pitching moment trends for the first generation 2DOF-TP. The L/D with the tilting/pivoting ducted fan vehicle has a low L/D (L/D~4) and is always lower than the L/D of the vehicle with just the wing (and no ducts). These results are for a modest cruise speed of 178knots or 300ft/s (M~0.27 at cruise at sea level) and, therefore, do not exhibit significant compressibility drag (as might be exhibited by the second generation vehicles at M~0.68 at V=675ft/s=400knots at an altitude of 25kFt). The wing is constant chord with aspect ratio of AR=4.5 and the total wing planform area is S=450 ft^2. This wing geometry was selected prior to the sizing analysis presented latter in this paper. Because of a lower wing aspect ratio, L/D results presented for first generation 2DOF-TP vehicle are lower than the L/D results presented for first generation PPT vehicle.

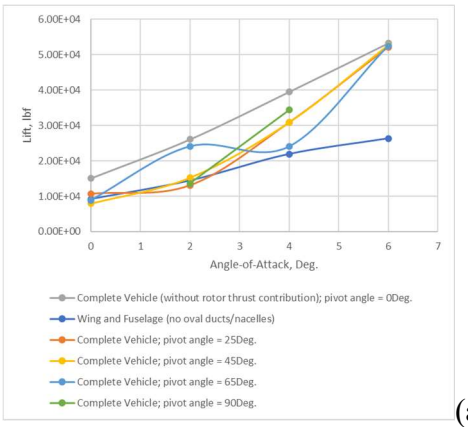

(a)

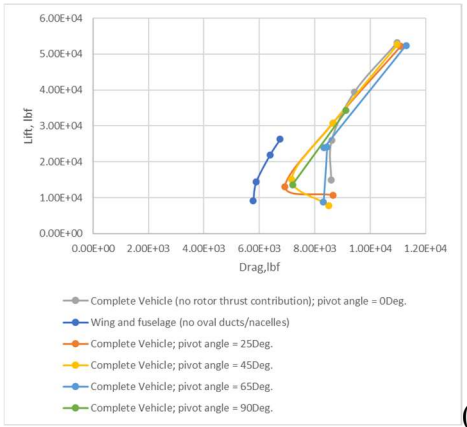

(b)

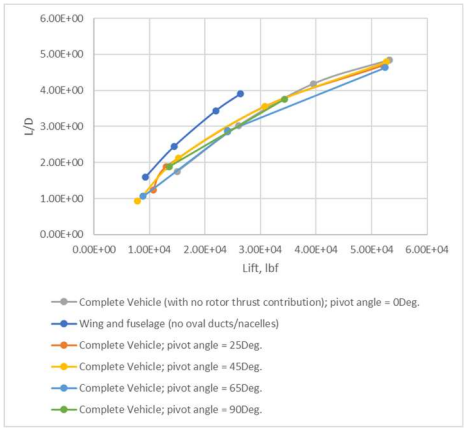

(c)

Figure 37. RotCFD predictions of first generation 2DOF-TP aerodynamic force trends: (a) lift curves; (b) drag polars; (c) total ducted fan thrust

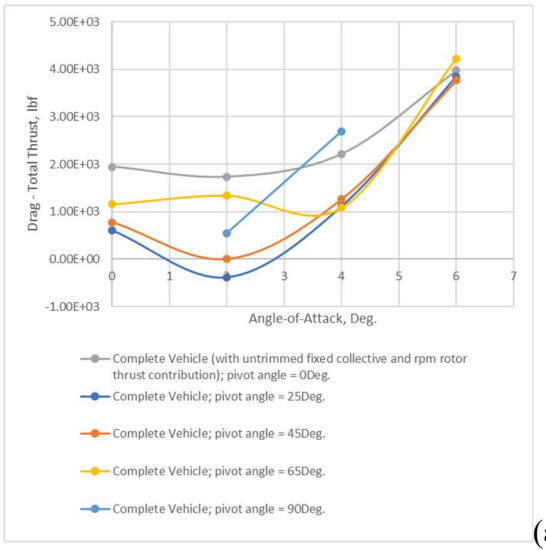

(a)

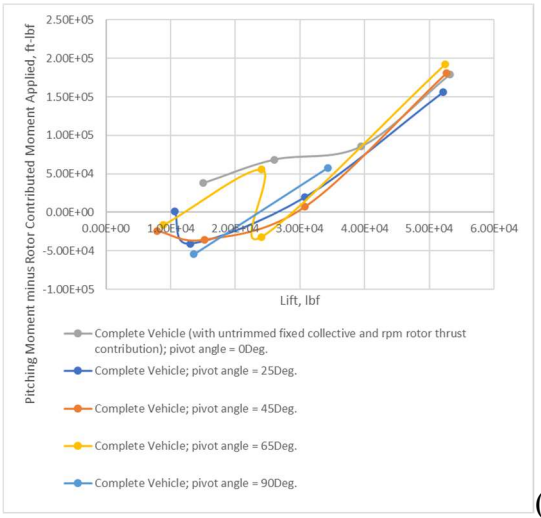

(b)

Figure 38. Untrimmed ducted-fan (a) thrust versus drag and (b) vehicle pitching moment

A second generation 2DOF pivoting and tilting ducted-fan vehicle configuration was shown earlier in Fig. 32. RotCFD predictions for this vehicle are shown in Figs. 39-40. The flow field predictions (including rotor wakes) are shown as velocity magnitude isosurfaces are generally consistent with the first generation vehicle – UAV or small aircraft – configuration results earlier shown in Figs. 34-35.

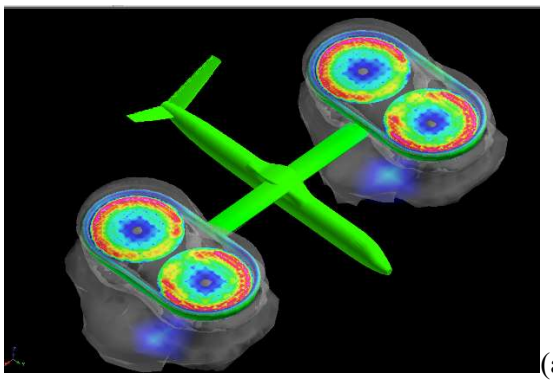

(a)

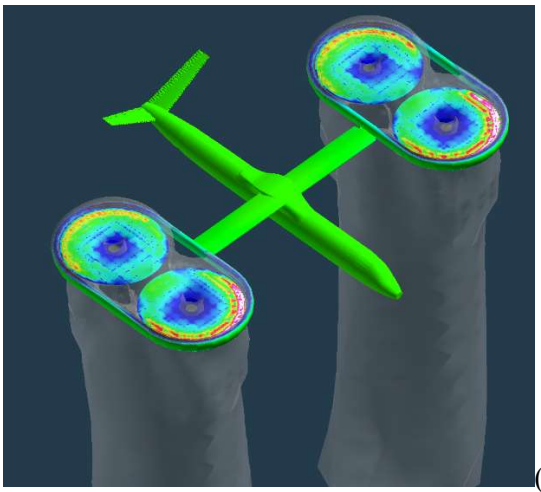

(b)

Figure 39. Hovering in and out of ground effect of second generation 2DOF tilting/pivoting ducted fan aerial vehicle and rotor wakes: (a) HIGE and (b) HOGE

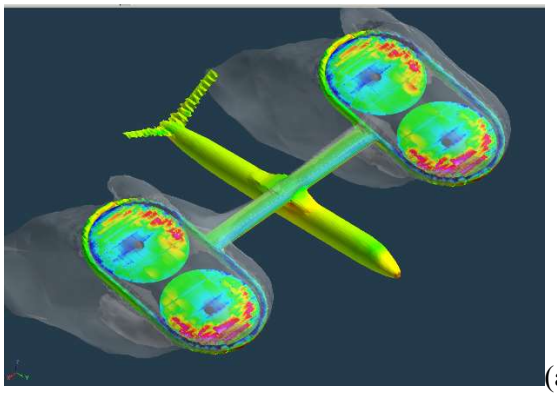

(a)

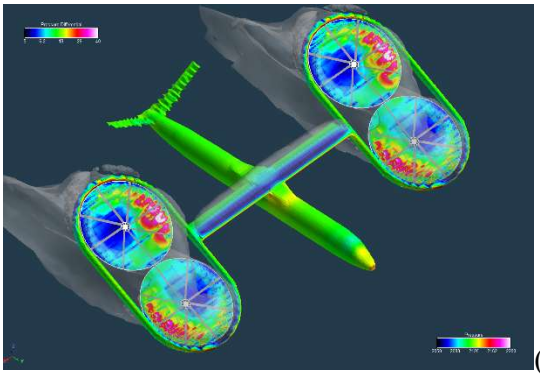

(b)

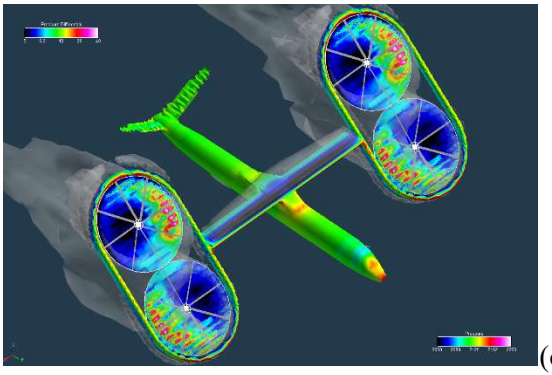

(c)

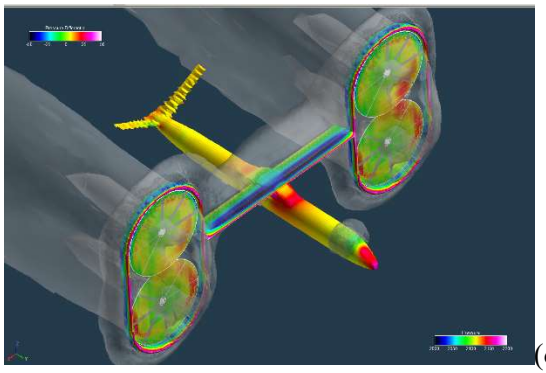

(d)

Figure 40. Hover and low-speed second generation 2DOF tilting/pivoting ducted fan aerial vehicle and rotor wakes: (a) V=100ft/s, i_N=75 Deg., i_P=0 Deg., and AOA=6 Deg.; (b) V=200ft/s, i_N=60 Deg., i_P=0 Deg. and AOA=4 Deg.; (c) V=250ft/s, i_N=45 Deg., i_P=0 Deg., and AOA=2 Deg.; V=300ft/s, i_N=0 Deg., i_P=0 Deg., AOA=4 Deg.

Some of the critical aerodynamic technical challenges for 2DOF-TP aircraft is as follows. First, detailed trade study (versus the very limited first order assessment performed in this paper) needs to be performed between the fixed-wing planform area and the pivoted ('horizontal') Oval duct's lifting area. Second, there is a clear trade between duct weight and accomplishing aero goals. Increasing hover duct thrust augmentation, low-speed helicopter-model pitch control trim (for oval ducts with embedded tandem fans), and even cruise drag considerations dictate larger ducts. Duct cross-sectional airfoil thickness and mean chord lengths are also important considerations to the overall weight/aero tradeoff. For example, the thicker duct cross-sectional airfoils for the second generation 2DOF-TP vehicle are great for hover thrust augmentation but bad for transition and high-speed flight because of very high drag levels. Third, if for reasons of vehicle pitching moment static trim control in hover and low-speed flight the fan-to-fan longitudinal spacing, x, needs to be $x/R>\pi$ then the better option is to have two circular ducts (resulting in an aircraft like the X-22) rather than continuing to try using an oval duct instead. If vehicle pitching moment static trim can be satisfactorily accomplished with $x/R<\pi$ then an oval duct is an acceptable approach. This is because an oval duct has less wetted area (if the same equivalent duct chord length is used for both) than two circular ducts if $x/R<\pi$. Note that all oval ducts studied in this paper have x/R=2 and, therefore, have less wetted area than the two equivalent (same radii) circular ducts.

The weight estimation methodology of 2DOF-TP builds upon the sizing analysis work discussed in Refs. 12 and 13 for single degree-of-freedom tilting ducted-fan aircraft. The current weight estimation work of this paper is a modest extension of that earlier work. Some of the unique weight estimate

aspects of the original ducted-fan work and the 2DOF-TP work in this paper is given as follows. First, there is a weight increase for the added degree-of-freedom for pivoting in addition to the tilt nacelle capability. This increase is likely dependent on the total nacelle pivoting to be provided for. A 25% increase in drive train weight to account for increased complexity and the inclusion of actuator/vane subsystems is assumed, as well as for accounting for the addition of a pivoting mechanism. Second, there is a weight increase for the ducts. This weight estimate is based on the specific duct configuration chosen, the number of ducts, and the perimeter mean chord length of the ducts.[3] This duct weight estimation methodology is detailed in Ref. 13. Third, there is a weight increase for any embedded movable vanes and/or streamlined supports inside the ducts for vehicle trim (if required) and for support of the motors and the tilting and pivoting mechanisms. Fourth, weight increases to provide for flaps on the duct exit (straight panel) edges to potentially provide for better total vehicle yaw control and static stability in yaw. Fifth, providing for one degree-of-freedom tilt capability will require an increase in vehicle tail volume and, therefore, represents a small fuselage weight increase. (This tail volume increase probably wasn't accounted for adequately in the Ref. 13 work but needs to be reflected in analyses going forward. A fuselage weight increase of 10% is assumed to account for tail volume increase to provide for improved vehicle pitching moment trim throughout transition/conversion.) Sixth, with the two degree-of-freedom pivoting capability, it might be possible to reduce some of the main fixed-wing weight because some of the pivoted oval ducts will be carrying a nonnegligible portion of the overall vehicle lift (a 5% wing weight reduction is assumed for the sizing analysis but further reductions for a thinner wing are not assumed to reflect that the duct weight must be carried). Seventh, a fixed equipment weight reduction of 50% is assumed to reflect fewer passengers than comparable gross weight conventional aircraft.

Table 14. First-order vehicle sizing for first generation (UAV/small-aircraft) 2DOF pivoting/tilting aircraft concept

Main Rotor Disk Loading	33.87	lbf/ft^2
Main Rotor Radius	2.06	ft
Number of Blades	8.00	Nondim.
Main Rotor Solidity	0.20	Nondim.
Main Rotor Tip Speed	781.53	ft/s
Nominal (Mean) Airplane-Mode Cruise Wing Loading	107.88	lbf/ft^2
Cruise Wing (Including Duct Planform) Area	35.71	ft^2
Number of Electric Motors per Rotor	1.00	Nondim.
Hover Power	404.42	Hp
Advance Ratio	0.21	Nondim.
Nominal Helicopter-Mode Forward Flight Power	283.24	Hp
Vehicle Effective Lift over Drag in Airplane-Mode Cruise	3.74	Nondim.
Nominal (Mean) Airplane-Mode Cruise Power	550.15	Hp
Energy from Battery over Total Mission Energy	0.08	Nondim.
Prescribed Fraction of Power Delivered by Electric Motors in Hover versus Turboshaft Engines	0.25	Nondim.
Prescribed Fraction of Power Delivered by Electric Motors in Helicopter-Mode Forward Flight versus Turboshaft Engines	0.25	Nondim.
Prescribed Fraction of Power Delivered by Electric Motors in Airplane-Mode Cruise versus Turboshaft Engines	0.00	Nondim.
Payload (and/or Passengers and Crew)	500.00	lbf
Total Weight of Rotors	135.59	lbf
Fuselage Weight	324.83	lbf
Wing Weight	329.60	lbf
Total Turboshaft Engines and Drive Train Weight	161.47	lbf
Total Fuel Weight	134.41	lbf
Total Battery Weight	247.57	lbf
Total Electric Motor Weight	383.14	lbf
Total Fixed Equipment Weight	130.04	lbf
Total Tilting Duct System Weight	129.06	lbf
Total TOGW =	2475.70	lbf

[3] It is assumed that the oval duct mean chord length is proportional to the overall duct planform dimensions. For the purposes of the sizing analysis, the following functional form is assumed: $c_{Duct} = cRe^{-b(R-1)}$ where b and c are constants and were assigned the values of c=0.35 and b=0.37. This gives $c_{Duct} = 0.35R$ for the first generation ducted-fan vehicle rotor radius and duct size, which is consistent with the duct mean chord length used in Ref. 13.

Table 15. First-order vehicle sizing for second generation (large, passenger-carrying regional) 2DOF pivoting/tilting aircraft concept

Main Rotor Disk Loading	33.87	lbf/ft^2
Main Rotor Radius	12.74	ft
Number of Blades	8.00	Nondim.
Main Rotor Solidity	0.20	Nondim.
Main Rotor Tip Speed	781.53	ft/s
Nominal (Mean) Airplane-Mode Cruise Wing Loading	100.12	lbf/ft^2
Cruise Wing (Including Duct Planform) Area	1024.49	ft^2
Number of Electric Motors per Rotor	1.00	Nondim.
Hover Power	13525.57	Hp
Advance Ratio	0.21	Nondim.
Nominal Helicopter-Mode Forward Flight Power	8392.73	Hp
Vehicle Effective Lift over Drag in Airplane-Mode Cruise	6.27	Nondim.
Nominal (Mean) Airplane-Mode Cruise Power	16706.01	Hp
Energy from Battery over Total Mission Energy	0.03	Nondim.
Prescribed Fraction of Power Delivered by Electric Motors in Hover versus Turboshaft Engines	0.25	Nondim.
Prescribed Fraction of Power Delivered by Electric Motors in Helicopter-Mode Forward Flight versus Turboshaft Engines	0.25	Nondim.
Prescribed Fraction of Power Delivered by Electric Motors in Airplane-Mode Cruise versus Turboshaft Engines	0.00	Nondim.
Payload (and/or Passengers and Crew)	12500.00	lbf
Total Weight of Rotors	7367.96	lbf
Fuselage Weight	19974.95	lbf
Wing Weight	9240.04	lbf
Total Turboshaft Engines and Drive Train Weight	8655.07	lbf
Total Fuel Weight	13141.33	lbf
Total Battery Weight	9241.63	lbf
Total Electric Motor Weight	9011.47	lbf
Total Fixed Equipment Weight	3510.72	lbf
Total Tilting Duct System Weight	1479.25	lbf
Total TOGW =	94122.43	lbf

The first-order sizing analysis presented is generally too preliminary to make engineering judgments as to which, if any, of the novel high-speed rotorcraft concepts presented in this paper are the 'best' vehicle configuration to pursue. Figures 41-42 are only presented in a very qualified sense.

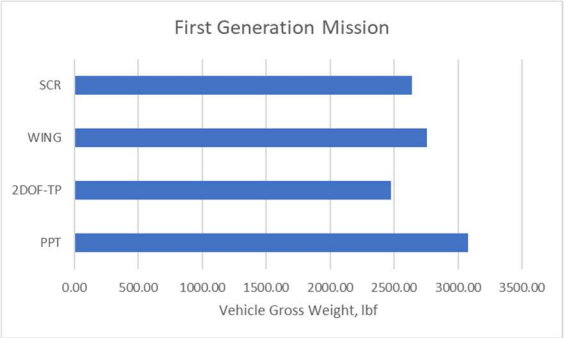

Figure 41. Gross weight of vehicle configurations meeting first generation mission profile

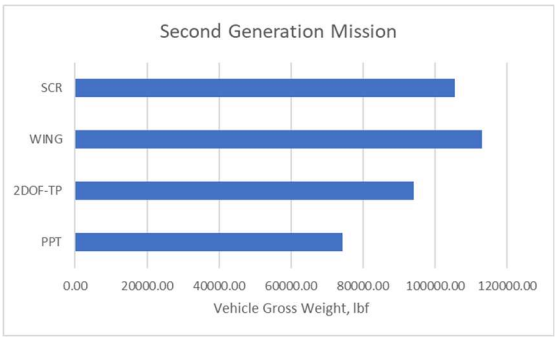

Figure 42. Gross weight of vehicle configurations meeting second generation mission profile

In general, not unexpectedly, stopped-rotor configurations are heavier than non-stopped-rotor high-speed rotorcraft. (This assumes that non-stopped-rotorcraft can embody technologies that will successfully allow proprotor/ducted-fan operation to greater than or equal to the 400knot threshold used in this paper.) Additionally, in general, incorporating 'sustainable aviation' hybrid-electric propulsion systems into high-speed rotorcraft designs will inevitably result in heavier aircraft and lower passenger counts than purely turboshaft and/or turbofan engine powerplant installations. Finally, differences in vehicle gross weight estimates between the novel configurations presented are less dramatic for the notional first generation mission and the second generation mission. Defining mission profiles that are consistent with future anticipated missions and applications will continue to be important drivers for future work in this area.

THRUST (Thrust-tilting High-speed Rotorcraft Uav for Science and Technology)

Technology demonstrators will be necessary to validate high-speed (400knot-plus) VTOL aircraft flight. This section of the paper discusses one possible approach to perform such high-speed rotorcraft

technology demonstrations cost-effectively. This approach is called for generally purposes of discussion in this paper as THRUST (Thrust-tilting High-speed Rotorcraft Uav for Science and Technology).

Current large-scale wind tunnels, such as the NASA Ames National Full-scale Aerodynamics Complex (NFAC) 40-by-80Ft. wind tunnel is only capable of reaching 300 knots maximum speed; clearly some other approach to performing high-speed rotorcraft demonstrations must be defined. Developing a flying full-scale vehicle with pilots onboard would seem to be a costly endeavor. Alternatively, it is proposed herein to focus on a small-scale demonstrator that uses a common/modular core that could be used for different high-speed rotorcraft concepts; refer to Fig. 43. This proposed use of small-scale systems and common/modular core approach to demonstrator development would hopefully result in less development costs.

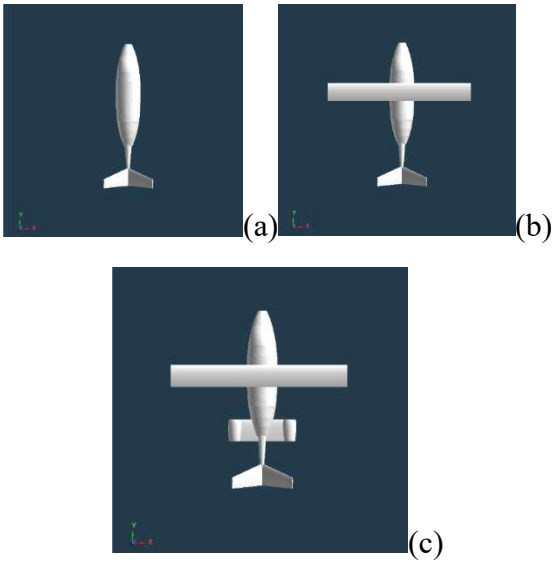

Figure 43. Notional common/modular core for THRUST demonstrator development: (a) common fuselage; (b) common fuselage and wing; (c) common fuselage, wing, and auxiliary propulsion

Another proposed approach to reduce demonstrator development and operational costs is to break up flight demonstrations into smaller phases of operation/demonstration. Further, it is also proposed that – like the NASA X-15 aircraft and other X-planes of the past – for the high-speed cruise demonstration phase the demonstrator would be released from a carrier aircraft. One example of an active aircraft that is specially tailored for the carrier aircraft role is the Boeing 747 noted in Ref. 43. Figures 44-46 illustrate one approach to breaking up the flight demonstration into different flight phases.

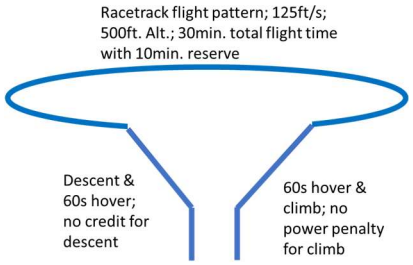

Figure 44. Notional THRUST demonstrator mission profiles: hover and low-speed flight

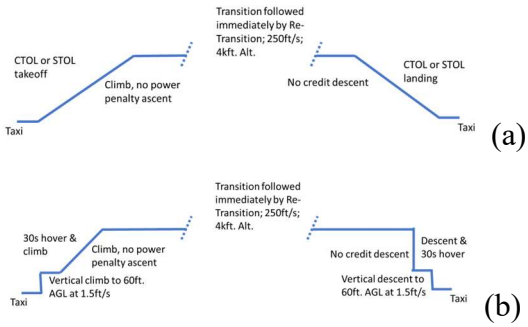

Figure 45. Notional THRUST demonstrator mission profiles: (a) stopped-rotor transition/conversion demonstrations; (b) non-stopped-rotor transition

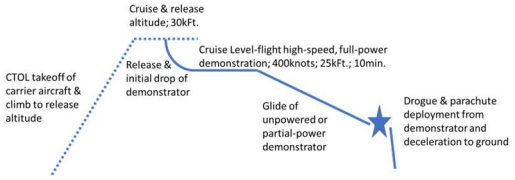

Figure 46. Notional THRUST demonstrator mission profiles: high-speed demonstration with notional use of carrier aircraft

Figure 47 illustrates the notional mounting of a THRUST high-speed rotorcraft demonstrator on a carrier aircraft. Space/volume envelope limitations will inevitably size the demonstrator aircraft that could be suspended/mounted and released from a Boeing 747 carrier aircraft. An alternate aircraft could be the Stratolaunch carrier aircraft, see Ref. 44; this aircraft would allow for potentially even larger-scale demonstrators to be tested, if deemed necessary.


(a)

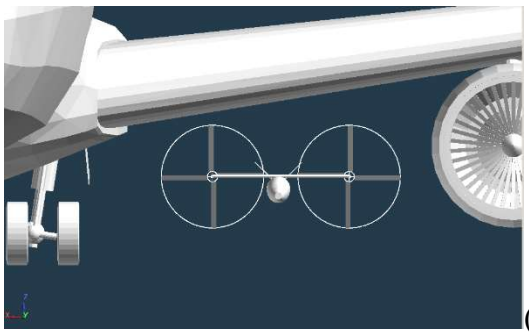
(b)

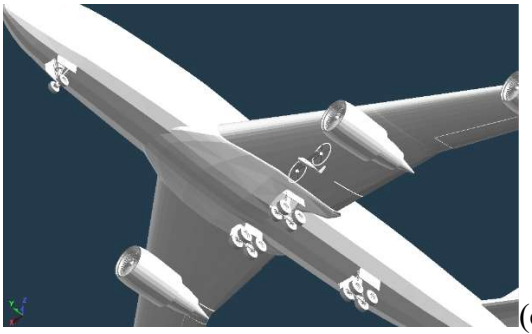
(c)

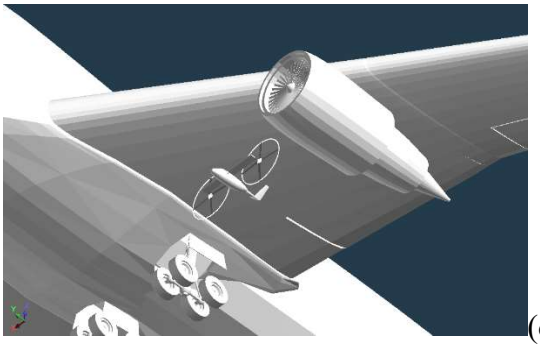
(d)

Figure 47. Use of carrier aircraft to cost-effectively, efficiently test at high cruise speeds THRUST demonstrators

The first generation WING and PPT conceptual design configuration geometries discussed earlier in the paper are both consistent with the notional THRUST common core module concept shown in Fig. 43.

FUTURE WORK

This paper is an introduction of four novel high-speed rotorcraft concepts. It will take a considerable amount of technical work in the future to sort through these – and other concepts – to arrive at one or two key candidate concepts to take into a more detailed technical assessment and technology development effort. The paper's goal is to be inspirational to a new generation of rotorcraft researchers and designers to one day develop practical and efficient 400knot plus high-speed rotorcraft and, thereby, expanding the overall application domain for all rotorcraft. This work outlines some of the

specific, critical high-speed rotorcraft technical challenges (and the limitations of the analysis tools available to address those technical challenges) that need to be overcome.

Table 16 is a summary list of some of the technical challenges to be faced in reexamining the design space for high-speed rotorcraft.

Table 16. High-speed rotorcraft technology challenges to be addressed by future work

	Priority	Tech Challenge	Work to Address
1	High	Develop and/or extend and experimentally validate new CFD and analysis tools capable of accurately predicting stopped-rotor transient aero and dynamic loads during conversion	Tool development and evaluation; small-scale foundational experiments
2	High	Develop and/or extend and experimentally validate new rotor/vehicle flight dynamic analyses examining stopped-rotor conversion and other phases of high-speed flight; such work should focus on variable geometry/configurations that significantly reconfigure throughout all phases of flight	Tool development
3	High	Develop and/or extend and experimentally validate new methodologies to examine whirl-flutter stability of novel proprotor and wing, or ducted-fan and wing, designs	Tool development and evaluation; foundational experiments
4	Moderate	Develop new optimal aeroperformance design approaches that consider heretofore unexplored rotor/vehicle trade spaces	Tool development and trade studies
5	Moderate	Systems analysis/engineering trade studies to better develop/refine mission concepts/applications for high-speed rotorcraft and to engage in analysis of alternatives	System analysis and trade studies
6	Moderate	New mechanical system concepts for nacelle tilt (and pivot) and flight controls	Design, prototyping, and test and evaluation
	Moderate	New mechanical system concepts for indexed-tip and embedded servo-flaps for rotors/proprotors to better be able to reconfigure rotor/proprotor twist for widely disparate low-speed and high-speed flight	Tool development, design, prototyping, and small-scale test and evaluation
7	High	Mechanical system and propulsion development to yield practical (light weight, high-power, and wide range of efficient operation) convertible engines and/or examine the relative trade space of all-combustion convertible engines against hybrid electric (batteries and turbogenerators) propulsion for high-speed rotorcraft applications/design	Tool development and design and computational evaluation; systems analysis and trade studies
8	High	Address through systems analysis the ‘big question’ of whether sustainable aviation goal is consistent with high-speed rotorcraft	Systems analysis/engineering trade studies
9	Moderate	Systems engineering trade space examination of relative tradeoffs of certain high-speed rotorcraft technologies for military missions versus civilian/commercial missions	Systems analysis/engineering trade studies
10	Moderate	Examine once again through systems analysis the relative tradeoffs of STOL versus VTOL for regional high-speed rotorcraft missions	Systems analysis/engineering trade studies
11	High	Encourage a new generation of aerospace engineers to seek efficient, productive, and sustainable high-speed rotorcraft to hopefully one day transform civilian/commercial aviation with an expansion of rotorcraft into all sectors of subsonic flight	Mission/vehicle conceptual design, trade studies, and foundational aerodynamics/aeromechanics evaluation

CONCLUDING REMARKS

Conventional tiltrotors are impressive aircraft. Nonetheless, current conventional tiltrotors are limited to cruise speeds just above 300knots. Previously proposed high-speed rotorcraft concepts to reach greater than or equal to 400 knots have not gained much traction towards to the development of practical aircraft, despite two to three decades of trying. New design approaches are needed.

Four different vehicle concepts – and two different sets of mission profiles – are described in the paper. Some initial aerodynamic analysis and vehicle sizing analysis are presented. Several technical challenges are described for both individual vehicle concepts and high-speed rotorcraft in general. Additionally, a sustainable aviation perspective is emphasized in this paper; all the vehicle concepts studied were assumed to employ a form of hybrid-electric propulsion.

This work can only be considered yet another small step forward with respect to one achieving practical, sustainable high-speed rotorcraft designs. A key aspect of this paper overall is to inspire others that follow to continue to work on this important problem in the future.

Author contact: Larry Young,
larry.a.young@nasa.gov

ACKNOWLEDGMENTS

This work is for Benton Lau and Anita Abrego (both formerly affiliated with NASA Ames Research Center; both, unfortunately, no longer with us). Their work – and their presence – was and still is an inspiration to their colleagues. This work makes extensive use of the mid-fidelity CFD software tool, RotCFD, which was developed by the late Professor R. Ganesh Rajagopalan, of Iowa State University and Sukra-Helitek. This CFD tool was developed, in part, by several NASA SBIR's and other government contracts. Finally, this is for my former NASA mentor, Robert H. Stroub, high-speed rotorcraft proponent and engineering innovator.

REFERENCES

[1] Edenborough, H.K., "Investigation of Tilt-Rotor VTOL Aircraft Rotor-Pylon Stability," *AIAA Journal of Aircraft*, Vol. 5, No. 6, March-April 1968.

[2] Swanson, A. A. and Light, J., "Shadowgraph Flow Visualization of Isolated Tiltrotor and Rotor/Wing Wakes," Proceedings of the 48th Annual Forum of the American Helicopter Society, June 1992.

[3] Young, L.A. and Derby, M.R., "Rotor/Wing Interactions in Hover," NASA TM 2002-211392, April 2002.

[4] Felker, F.F., Young, L.A., and Signor, D.B., "Performance and Loads Data from a Hover Test of a Full-Scale Advanced Technology XV-15 Rotor," NASA TM 86854, January 1986.

[5] Felker, F.F. Signor, D, Young, L.A., and Betzina, M., "Performance and Loads Data From a Hover Test of a 0.658-Scale V-22 Rotor and Wing," NASA TM 89419, April 1987.

[6] Young, L. A., "Tilt Rotor Aeroacoustic Model (TRAM): A New Rotorcraft Research Facility," American Helicopter Society (AHS) International Specialist's Meeting on Advanced Rotorcraft Technology and Disaster Relief, Gifu, Japan, April 1998.

[7] Young, L. A., Booth, E. R., Yamauchi, G. K., Botha, G., Dawson, S.,

"Overview of the Testing of a Small-Scale Proprotor," 55th Annual Forum of the American Helicopter Society, Montreal, Canada, May 25-27, 1999.

[8] Johnson, J.L. and Young, L.A., "Tilt Rotor Aeroacoustic Model Project," Confederation of European Aerospace Societies (CEAS) Forum on Aeroacoustics of Rotors and Propellers, Rome, Italy, June 9-11, 1999.

[9] Young, L.A., Lillie, D., McCluer, M., Derby, M., and Yamauchi, G.K., "Insights into Airframe Aerodynamics and Rotor-on-Wing Interactions from a 0.25-Scale Tiltrotor Wind Tunnel Model," AHS International Specialists Meeting on Aerodynamics, Acoustics, and Test and Evaluation, San Francisco, CA, January 21-23, 2002.

[10] DARPA SPRINT project; https://www.defensedaily.com/darpa-taps-four-firms-for-sprint-program-to-develop-high-speed-vtol-x-planes/advanced-transformational-technology/; last accessed December 8, 2023.

[11] Young, L.A., "What is a Tiltrotor? A Fundamental Reexamination of the Tiltrotor Aircraft Design Space," AHS International Technical Meeting on Aeromechanics Design for Transformative Vertical Flight, San Francisco, CA, January 16-18, 2018.

[12] Young, L.A., Aiken, E.W., Derby, M.R., Johnson, J.L., Navarrete, J., and Demblewski, R., "Engineering Studies into Vertical Lift Planetary Aerial Vehicles," AHS International Meeting on Advanced Rotorcraft Technology and Life Saving Activities, Utsunomiya, Tochigi, Japan, November 11-13, 2002.

[13] Young. L.A., "Novel Tilting Ducted-Fan Aerial Vehicle Configurations," 10th Autonomous VTOL Technical Meeting and 10th Annual Electric VTOL Symposium, Mesa, AZ, January 24-26, 2023.

[14] Gibson, T.; Jagielski, M.; Barber, J., Chung. W., and Young, L., "Employment of Conceptual Civil Tiltrotor Aircraft in Disaster Response," 68th Annual Forum of the AHS International, Fort Worth, TX, May 1-3, 2012.

[15] Young, L.A., "Future Roles for Autonomous Vertical Lift in Disaster Relief and Emergency Response," Heli-Japan 2006: AHS International Meeting on Advanced Rotorcraft Technology and Life Saving Activities, Nagoya, Japan, November 15-17, 2006.

[16] Johnson, W., Lau, B.H., and Bowles, J.V., "Calculated Performance, Stability, and Maneuverability of High-Speed Tilting-Prop-Rotor Aircraft," NASA TM 88349, September 1986.

[17] Soule, V.A., "V/STOL Tilt Rotor Aircraft Study (Volume V)," NASA CR 114598, March 1973.

[18] Wolkovitch, J., Wainfan, B., Ben-Harush, Y., and Johnson, W., "Application of the Joined Wing to Tiltrotor Aircraft," NASA CR 177543, November 1989.

[19] Rajagopalan, R.G., Baskaran,V., Hollingsworth, A., Lestari, A., Garrick, D., Solis, E., Hagerty, B., "RotCFD - A Tool for Aerodynamic Interference of Rotors: Validation and Capabilities", AHS Future Vertical Lift Aircraft Design Conference, January 18-20, 2012 San Francisco.

[20] Rajagopalan, G., Thistle, J., Polzin, W., "The Potential of GPU Computing for Design in RotCFD," AHS Technical

Meeting on Aeromechanics Design for Vertical Lift, Holiday Inn at Fisherman's Wharf, San Francisco, CA, January 16-18, 2018.

[21] Young, L.A., "Asymmetry in Rotorcraft Design," NASA TM (Soon to be published).

[22] Young, L.A., "Performance, Inflow, and Tip Loss Characteristics of Rotors with Discontinuous Steps in Twist and Lift at their Blade-Tips," NASA/TM-2022-0017246, February 2023.

[23] Acree, C.W., "Integration of Rotor Aerodynamic Optimization with Conceptual Design of a Large Civil Tilt Rotor," Presented at the American Helicopter Society Specialists' Conference on Aeromechanics, January 20-22, 2010.

[24] Young, L.A., "A Transportation and Habitation System Architecture enabled by Multi-Modality Mobility Platforms," NASA TM (Soon to be published).

[25] Eisenberg, J.D., "The Selection of Convertible Engines with Current Gas Generator Technology for High Speed Rotorcraft," NASA TM 103774.

[26] McArdle, J.G., Barth, R.L., Wenzel, L.M., and Biesiadny, T.J., "Dynamic and Transient Performance of Turbofan/Turboshaft Convertible Engine With Variable Inlet Guide Vanes," NASA TM 4696, April 1996.

[27] Young, L.A., "Urban Aerial Mobility Networks using Amphibious Vertical Takeoff and Landing Vehicles," 9th Biennial Autonomous VTOL Technical Meeting & 8th Annual Electric VTOL Symposium, Jan. 26–28, 2021.

[28] Schatzman, N., Dominguez, M., Lee, P., and Young, L.A., "LILI (Long-term Ice-field Levitating Investigator): Mars Aerial and Ground Explorer for Martian Polar Regions," Vertical Flight Society Transformative Vertical Flight Conference, San Jose, CA January 25-27, 2022.

[29] Young, L.A., "Rotorcraft as Robots," NASA TM (soon to be published).

[30] Husseyin, S., "Design Considerations for a Stopped-Rotor Cyclocopter for Venus Exploration," ARC-E-DAA-TN34484-2, October 24, 2016; https://ntrs.nasa.gov/citations/20160012563; last accessed December 8, 2023.

[31] Large 'conventional' (axis of rotation normal to flight path) cycloidal rotor demonstrator vehicle; https://www.cyclotech.at/; last accessed November 20, 2023.

[32] Benedict, M., Jarugumilli, T., Chopra, I., "Experimental Optimization of MAV-Scale Cycloidal Rotor Performance," *Journal of the American Helicopter Society*, Volume 56, Number 2, 1 April 2011, pp. 22005.

[33] Benedict, M., Ramasamy, M., Chopra, I., Leishman, J. G., "Performance of a Cycloidal Rotor Concept for Micro Air Vehicle Applications," *Journal of the American Helicopter Society*, Volume 55, Number 2, 1 April 2010, pp. 22002.

[34] Benedict, M., Ramasamy, M., and Chopra, I., "Improving the Aerodynamic Performance of Micro-Air-Vehicle-Scale Cycloidal Rotor: An Experimental Approach," *Journal of Aircraft*, Vol. 46, No. 4, July-August 2010.

[35] Sirohi, J, Parsons, E., Chopra, I., "Hover Performance of a Cycloidal Rotor for a Micro Air Vehicle," *Journal of the American Helicopter Society*, March 2007.

[36] Betz, A., “The Ground Effect on Lifting Propellers,” NACA TM #836, August 1937.

[37] Abrego, A., and Bulaga, R., "Performance Study of a Ducted Fan System," Proceedings of the AHS Aerodynamics, Acoustics, and Test and Evaluation Meeting, San Francisco, California, January 23-25, 2002.

[38] Zhang, T. and Barakos, G. N., “Review on ducted fans for compound rotorcraft,” *Aeronautical Journal*, 124, 2020, pp. 941-974.

[39] Johnson, W., "NDARC: NASA Design and Analysis of Rotorcraft Theory," NASA/TP–20220000355/Vol 1.

[40] Johnson, W., “NDARC: A Tool for Synthesis and Assessment of Future Vertical Lift Vehicles,” *Vertiflite*, Published by AHS International, November-December 2014; https://vtol.org/news/november-december-2014-vertiflite-now-online; last accessed July 21, 2017.

[41] Embraer E-195 GE CF34-10E engines; https://www.aerospace-technology.com/projects/embraer-e-195-commercial-regional-jet/; last accessed November 20, 2023.

[42] Raymer, Daniel, *Aircraft Design: a Conceptual Approach, 3rd Edition*, AIAA Education Series, American Institute of Aeronautics and Astronautics, Reston, VA, 1999.

[43] Boeing 747 Carrier Plane; https://aviationweek.com/defense-space/aircraft-propulsion/stratolaunch-adds-747-400-air-launch-fleet; last accessed December 6, 2023.

[44] Stratolaunch “Roc’ Carrier Aircraft; https://www.stratolaunch.com/vehicles/roc/; last accessed December 8, 2023.

[45] Theodore, C., Willink, G., Amy, A., Russell, C., Pete, A., "Wind Tunnel Testing of a 1/20th Scale Large Civil Tilt-Rotor Model in Airplane and Helicopter Modes", AHS Fifth Decennial Aeromechanics Specialists' Conference, San Francisco, California, January 22-24, 2014.